Investigation of a Phased Array of Circular Microstrip Patch Elements Conformal to a Paraboloidal Surface

Sharath Kumar

Thesis submitted to the faculty of the
Virginia Polytechnic Institute and State University
in partial fulfillment of the requirements for the degree

Master of Science
In
Electrical Engineering

Dr. Amir I. Zaghloul, Chair
Dr. William A. Davis
Dr. Lamine M. Mili

September 11th, 2006
Falls Church, Virginia

Keywords: Paraboloidal Arrays, Conformal Arrays,
Circular Microstrip Patch Arrays

Investigation of a Phased Array of Circular Microstrip Patch Elements Conformal to a Paraboloidal Surface

Sharath Kumar

Abstract

This thesis investigates the performance of a phased array of antenna elements conforming to a paraboloidal surface. We hypothesize that such a conformal phased array would have performance comparable to that of a correspondingly sized planar array. The performance of a paraboloidal array of antenna elements was simulated using an array program, and the resulting gains, side-lobe levels, and half-power beamwidths compared to those of a similarly sized planar array. Furthermore, we propose a beam-forming feed network for this paraboloidal phased array, and discuss the influence that coupling between the elements could have on the array performance. Lastly, we propose that such an array be used in conjunction with a parabolic reflector antenna to form a versatile hybrid antenna with several potential applications.

Acknowledgments

I would like to take this opportunity to earnestly thank Dr. Amir I. Zaghloul, my advisor, for his patient guidance and support in making this work possible. I also wish to acknowledge the help of Maryam Parsa, who contributed to various aspects of this work. Lastly, I would like to thank the faculty of Virginia Tech for making the experience of graduate school enriching and fulfilling.

Contents

List of Figures and Tables

Chapter 1. Introduction

1.1 Motivation and Background

Antennas are a fundamental component of any wireless communication system. The ubiquity of wireless and satellite communications has spurred the development of an extraordinary range of antenna shapes and sizes, each with its own advantages and limitations. However, there are many applications where space is at a premium, and where there is an urgent need for an antenna with the flexibility to efficiently combine the capabilities of multiple antennas.

This thesis constitutes the groundwork and the first step in a broader proposal to model, simulate, analyze, design, build, and test a novel antenna that addresses the aforementioned need. This antenna, which we have dubbed the Hybrid Reflector-Array Antenna, is expected to be much more flexible than a conventional parabolic reflector, and will essentially pack the functionalities of two antennas, a parabolic dish and a phased array of paraboloidal shape, into the space of one. The Hybrid antenna will be comprised of two constituent antennas: a microstrip patch array conformal to a paraboloid, and a standard Cassegrain dual reflector antenna. The microstrip patch array is located in front of the reflector dish, and the two antennas operate simultaneously as one.

In modeling, simulating, and analyzing the Hybrid antenna, we realized that the best approach would be to first separately assess the constituent phased array and parabolic dish antennas, and then combine them to determine how they would perform when operated in unison. Of the two antennas that the Hybrid is comprised of, the phased array is the more difficult to accurately model and analyze, particularly due to its conformal nature. To the best of our knowledge, a complete and rigorous modeling and analysis of an array of microstrip patch elements conforming to a paraboloidal surface has not been done before.

1.2 Objective

This thesis aims to model, simulate, and analyze the operation of a phased array comprised of circular microstrip patch elements conforming to a paraboloidal surface, as part of a larger effort to determine its performance and behavior in a Hybrid antenna configuration. As a

constituent of the proposed Hybrid antenna, the array must have favorable gain and scanning characteristics.

1.3 Brief Description of Array

This thesis presents the simulation results of a hexagonal array of microstrip patches placed conformal to a paraboloidal surface. The phased array that will constitute part of the Hybrid antenna will be circular in shape and not hexagonal; however, we used the hexagonal array as an approximation to the circular paraboloidal array, and the results that we obtain using a hexagonal array should be applicable to a circular array as well.

As an example, the array that is analyzed in this thesis is comprised of 37 circular microstrip patch antennas arranged conformal to a paraboloidal surface, and in a hexagonal configuration. All simulations were conducted using the Array Program software, "ARRAY" [1]. We limited the number of elements in the array to 37 so as to reduce the duration of the task of computing location and orientation parameters for each element and to reduce simulation time. Furthermore, the conclusions that we draw from the 37 element array case will hold for larger arrays as well.

1.4 Organization of Thesis

This thesis is arranged as follows. Chapter 2 presents background information on conformal microstrip antenna arrays. Section 2.1 begins with a discussion of array theory, and presents the principles and the array factor equations that govern the operation of the general case of three-dimensional arrays. The concept of pattern multiplication, which is fundamental to array theory, is briefly discussed. Section 2.2 describes the principles of microstrip antenna radiation. The far field equations for a circular microstrip patch antenna are presented. Section 2.3 briefly discusses microstrip patch arrays. Chapter 3 defines the physical configuration of the paraboloidal array. We provide a detailed description of the physical layout and configuration of the paraboloidal array, including the parameters of the microstrip antenna elements. Chapter 4 provides a discussion of the expected performance of the paraboloidal array based on antenna theory. Section 4.1 addresses various aspects of the array's performance, such as gain, efficiency, and half-power beamwidth. Section 4.2 enters into a description of the expected scanning and phase quantization behavior of the

paraboloidal array. Chapter 5 presents extensively the simulation results obtained with scanning, and analyze them in detail. Section 5.1 addresses the case where no phase quantization is performed, and Section 5.2 assumes different levels of phase quantization to determine its influence on the array performance. Section 5.3 summarizes some of the important results obtained through simulation. Chapter 6 addresses the issue of mutual coupling in the paraboloidal array. Section 6.1 provides some background information on mutual coupling, Section 6.2 discusses mutual coupling effects in a planar microstrip array, and Section 6.3 focuses on the mutual coupling mechanisms in a conformal array, such as the paraboloidal array. Actual analysis and simulation of the mutual coupling in the paraboloidal array are not done within this work but are the subject of proposed future work. Chapter 7 addresses the need for a beam-forming feed network for the paraboloidal array. Section 7.1 provides background information on the topic of designing feed networks. Section 7.2 presents the feed network that we designed for the paraboloidal array, with detailed schematics of the proposed network. Chapter 8 concludes with a brief discussion of intended future work, wherein the paraboloidal array will be combined with a parabolic reflector antenna to form a hybrid antenna with many potential applications.

Chapter 2. Background: Microstrip Antenna Arrays

2.1 Array Theory

Multiple antennas can be interconnected by means of a feed network to form an array and made to work in concert to produce a more directional radiation pattern. Since the radiation pattern of an array is dependent on the summation of the far fields produced by the constituent elements, we can design a high-gain antenna array by interconnecting a number of relatively low-gain antenna elements.

It is important to distinguish between two types of arrays- those with similarly oriented, identical elements, and those with either dissimilar elements or elements with different orientations. The radiation pattern of an array of identical elements is the product of two parts- the pattern of each individual element (called the element pattern), and the array pattern that would result if the elements were isotropic radiators (also called the array factor).

$$F(\theta,\varphi) = g_a(\theta,\varphi)\, f(\theta,\varphi) \qquad (1)$$

In the above equation, $F(\theta,\varphi)$ is the overall, normalized pattern of the array, $g_a(\theta,\varphi)$ is the normalized element pattern, and $f(\theta,\varphi)$ is the normalized array factor.

The above principle, known as pattern multiplication, is fundamental to the operation of arrays. Pattern multiplication, however, is not applicable to arrays comprised of elements with dissimilar orientations, since the factorization of the overall pattern into the element and array factors is then not possible.

We now present the array factor equation for a three dimensional array, which will be instructive to us in understanding the behavior of the paraboloidal array. Consider the general case of an arbitrarily configured three dimensional array comprised of similar elements, with the elements arranged in a rectangular grid. A two dimensional (planar) analog of such an array, reproduced from [2], is shown below for convenience.

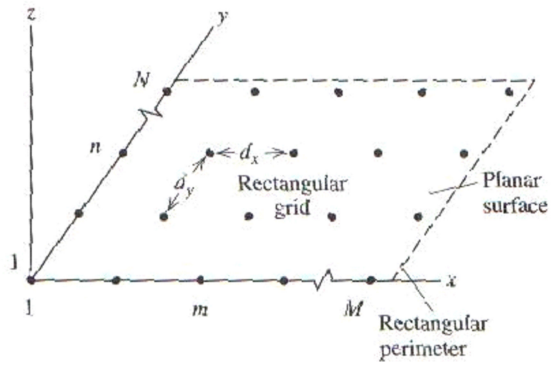

Figure 2.1. Planar Array of Elements

Figure 2.1 shows a planar array; however, we are considering the general case of a three dimensional array, such as a conformal array. Note that the elements are arranged in a rectangular grid, so that we can specify a particular element by its address, "mn". A vector that defines the position of each element in an arbitrary three dimensional array extends from the origin to the element with location "mn", and is given by [2]:

$$\mathbf{r'_{mn}} = x'_{mn}\,\mathbf{a_x} + y'_{mn}\,\mathbf{a_y} + z'_{mn}\,\mathbf{a_z} \qquad (2)$$

The array factor for a three dimensional array is given by the following summation [2]:

$$AF(\theta,\varphi) = \Sigma_{n=1\ to\ N}\,\Sigma_{m=1\ to\ M}\, I_{mn}\, e^{j(\beta\,\mathbf{a_r}\cdot\mathbf{r'_{mn}} + \alpha_{mn})} \qquad (3)$$

In the equation above, α_{mn} is the excitation current phase that is responsible for scanning or steering the main beam of the array.

In the case of a three dimensional array in which the elements are either dissimilar or differently oriented, the factoring of the overall pattern into an array factor and an element factor is not possible. The overall pattern is then simply the sum of the far field of each element constituting the array.

Antenna arrays are inherently more flexible than conventional antennas, and we can exercise far more control on the radiation pattern, whether in terms of beam scanning or for beam shaping purposes. As illustrated by the array factor equation above, we can implement a phase difference in the currents feeding adjacent elements to steer the array main beam to any desired angle. Additionally, we can reduce side-lobe levels in the array pattern by implementing amplitude tapering in the currents. The radiation pattern of an array is thus determined by the number and type of constituent antenna elements, their

spatial locations and orientations, and the amplitudes and phases of the currents feeding them.

Arrays come in several geometrical configurations. The most common are linear arrays and planar arrays. Linear arrays have elements arranged in a straight line, and planar arrays have elements arranged on a flat surface, such as a rectangular or hexagonal surface. Conformal arrays have the elements arranged on a curved, three-dimensional surface, such as a paraboloid. In a conformal array, the phases of the currents feeding the elements must be adjusted so that the radio waves on a plane in the far field all have the same phase (i.e., a plane wave).

2.2 Circular Microstrip Patch Antennas

Let us first discuss some chief features of microstrip antennas. Microstrip antennas have low bandwidths, typically only a few percent. Since microstrip antennas are resonant in nature, their required size becomes inconveniently large at lower frequencies. They are thus typically used at frequencies between 1 and 100 GHz. Microstrip antennas are relatively low-gain antennas. Their end-fire radiation characteristics and power-handling capability are relatively poor. However, microstrip antennas have several advantages as well, such as low cost, ease of construction, low profile design, and suitability in conformal array applications.

Microstrip patches can be square, rectangular, circular, triangular, elliptical, or any other common shape to simplify analysis and performance prediction.

A microstrip patch antenna consists of two parallel conductors separated by a thin layer of dielectric substrate. The lower conductor functions as a ground plane and the upper conductor acts as a patch antenna. Figure 2.2, reproduced from [3], is a circular microstrip patch antenna with radius R, substrate thickness h, and a dielectric relative permittivity ϵ_r.

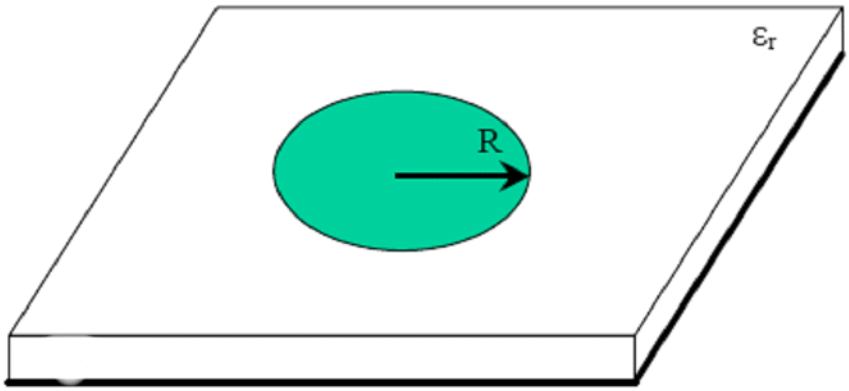

Figure 2.2. Circular Microstrip Patch Antenna

Microstrip antennas radiate due to the fringing fields between the patch and the ground plane. Figure 2.3, reproduced from [4], shows the fringing fields in a microstrip patch antenna.

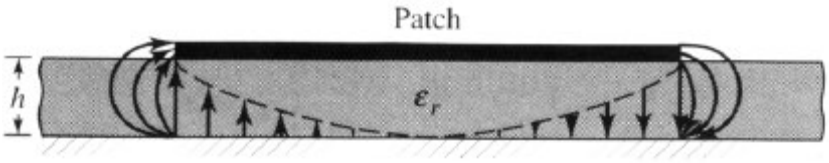

Figure 2.3. Fringing Fields in Microstrip Antenna

Multiple modes can be excited in a circular microstrip patch antenna, and the resulting far field electric field θ and φ components can be shown to be as follows [5]:

$$E_\theta^{(n)} = e^{jn\pi/2} (V_0^{(n)} / 2)\ k_0 R (J_{n+1} - J_{n-1}) \cos n(\varphi - \varphi_0)$$
$$E_\varphi^{(n)} = -e^{jn\pi/2} (V_0^{(n)} / 2)\ k_0 R (J_{n+1} + J_{n-1}) \cos\theta \sin n(\varphi - \varphi_0) \qquad (4)$$

In these equations, V_0 is the input voltage, k_0 is the wavenumber, $J_n = J_n (k_0 R \sin\theta)$ is the Bessel function of the second kind and order n, R is the radius of the patch, and φ_0 is the angle corresponding to the feeding point of the antenna.

Due to the fringing fields between the patch and the ground plane, the effective dimensions of the antenna are greater than the actual dimensions. The effective radius of the patch is related to the physical radius of the patch by [6]:

$$r_{eff} = R\,[1 + (2h/(\pi R \varepsilon_r))\,\{\ln(R/(2h)) + (1.41\,\epsilon_r + 1.77) + (h/R)\,(0.268\epsilon_r + 1.65)\}]^{1/2} \quad (5)$$

where R is the physical radius of the patch and h is the height of the dielectric substrate.

The resonant frequency of a microstrip patch antenna is dependent on the effective patch radius, and is given by [6]:

$$f_r = (c\,\alpha_{nm}) / (2\,\pi\,r_{eff}\,\sqrt{\varepsilon_r}) \quad (6)$$

where c is the velocity of light, r_{eff} is the effective radius of the circular patch, and α_{nm} are the zeros of the derivative of the Bessel function J_n (x). m and n specify the mode that is being considered. For the fundamental resonating TM_{11} mode, for example, the above equation produces [6]:

$$f_r = (c\,1.8412) / (2\,\pi\,r_{eff}\,\sqrt{\varepsilon_r}) \quad (7)$$

Shown in Figure 2.4 are some typical E-Plane and H-Plane patterns, taken from [4], for a circular patch antenna; three plots are to be found on each pattern: the first resulting from measurement, the second obtained theoretically using the Moment Method, and the third likewise obtained using a Cavity model.

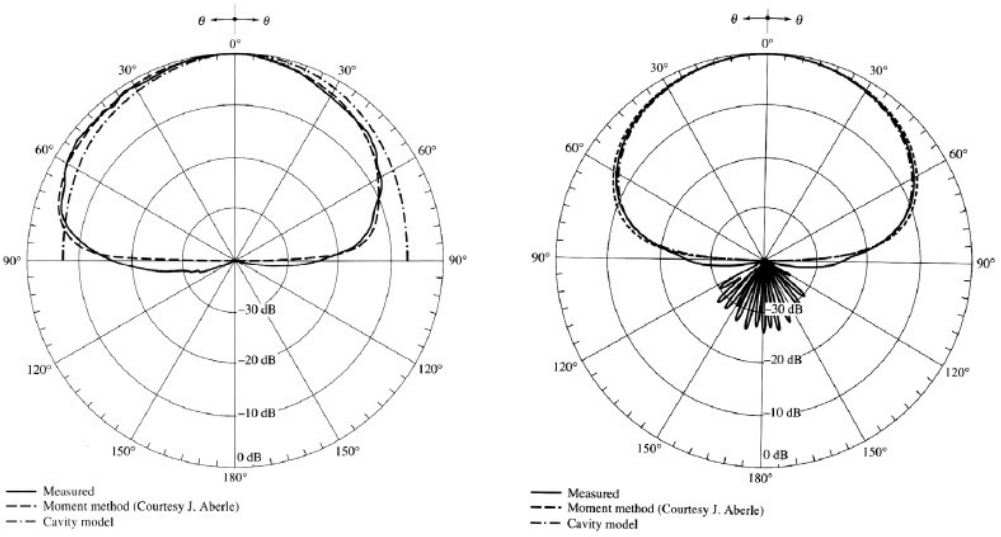

Figure 2.4. Typical E-Plane and H-plane Circular Microstrip Patch Patterns

2.3 Microstrip Arrays

Microstrip antenna arrays offer the advantage that the elements can be printed easily and at low cost on a flexible dielectric substrate. Such arrays are ideally suited for any application that calls for the design of low-profile, conformal antennas. Additionally, we can integrate microstrip radiating elements and feed networks with the transmitting and receiving circuitry. Microstrip antennas can be conveniently fed by microstrip lines in a number of different configurations. We can implement interelement spacings of less than the free-space wavelength to avoid grating lobes, but greater than half the free-space wavelength to provide sufficient room for the feed lines, to achieve higher gain for a given number of elements, and to reduce mutual coupling.

Figure 2.5 shows a planar microstrip array comprised of circular microstrip patches in a circular configuration.

Figure 2.5. Planar Array of Circular Microstrip Patches in Circular Configuration

Chapter 3. The Paraboloidal Array-Parameters and Configuration

We now describe the paraboloidal microstrip antenna array that is the subject of this thesis. The array consists of 37 circular microstrip patch antennas in a hexagonal configuration, and conforming to a paraboloidal surface. Following (Figure 3.1) is a diagram depicting the configuration of the elements as seen using the Array Program Software, "ARRAY". Note that it is a two-dimensional projection of the three-dimensional paraboloidal array. The hexagonal configuration is on the projection of the array grid on the x-y plane.

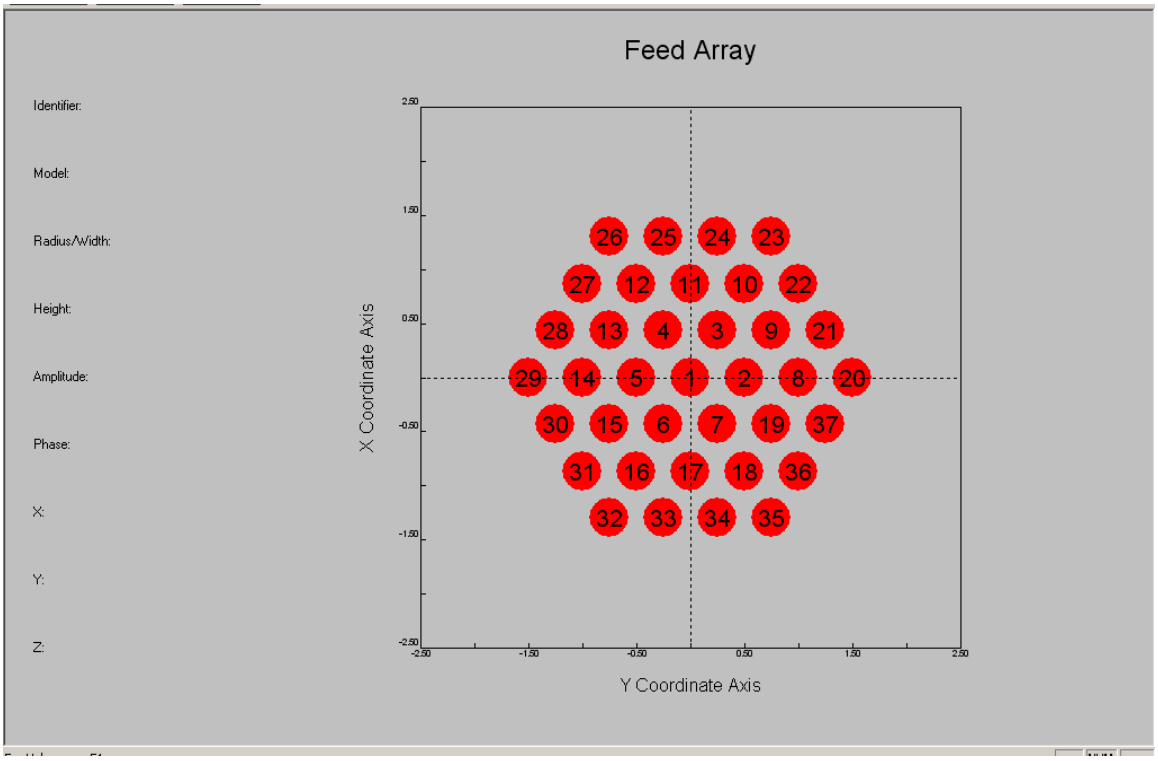

Figure 3.1. Snapshot of Paraboloidal Array as Seen on Software

The above projection of the array is, in fact, an idealization, since the curvature of the paraboloidal surface would distort the non-center circular patches into ellipses in an accurate projection.

The following are the parameters of the paraboloidal array and its constituent microstrip antennas. When projected onto a plane, the microstrip patches are arranged in a hexagonal configuration with interelement spacings in the y direction of half a wavelength

and interelement spacings of 0.433 wavelengths in the x direction. This makes for an inter-element spacing of 0.5 wavelengths, when the elements are projected onto a plane. Note that the curvature imposed by the three dimensional nature of the paraboloid implies that the elements are not equally spaced on the paraboloidal surface; the spacings increase away from the center. The diameter of each element is 0.375 wavelengths, which means that the diameter of the hexagonal configuration is 3.375 wavelengths.

Shown in Figure 3.2 is a more accurate two-dimensional projection of the paraboloidal array. The projections of the centers of the patches are on a hexagonal grid as described above. The projections of the patches are elliptical.

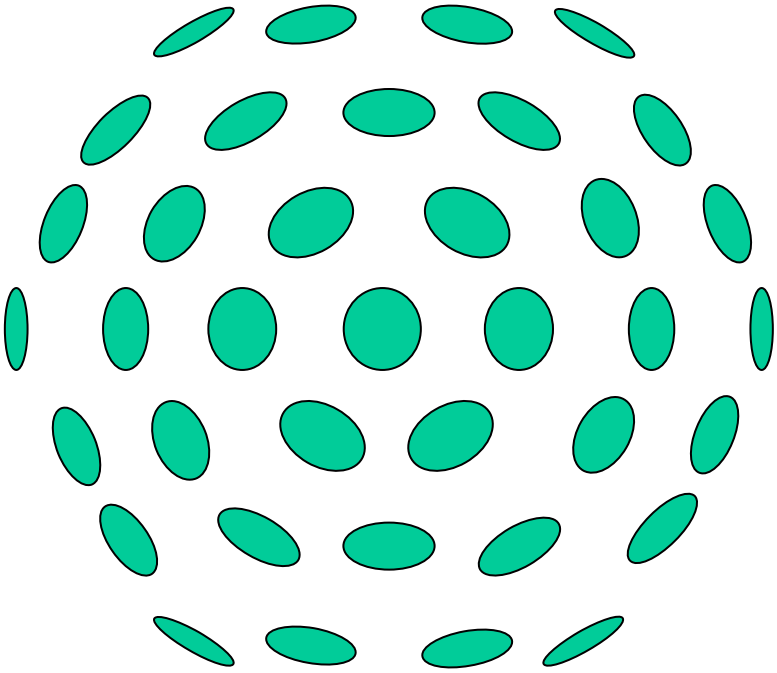

Figure 3.2. Two-Dimensional Projection of Paraboloidal Array

The lateral, parabolic curvature of the array is depicted in Figure 3.3. Note that the inter-element spacings on the parabolic surface increase away from the center.

Figure 3.3. Lateral Curvature of Paraboloidal Array

Figure 3.4 shows both the figure above and its projection, to make clear the fact that because the inter-element spacings in the projected array are constant, the inter-element spacings in the parabolic array are not; they increase radially due to the curvature of the surface.

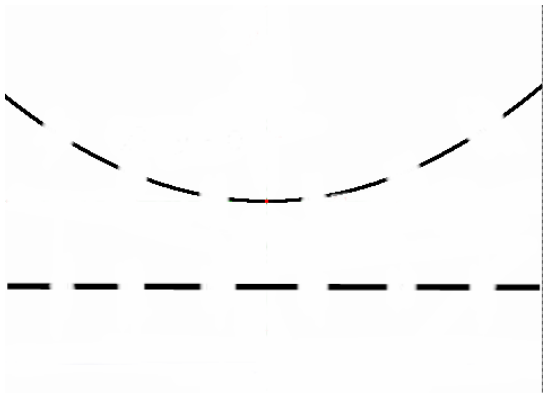

Figure 3.4. Illustration of Uneven Inter-element Spacings in Paraboloidal Array

In this example, the dielectric thickness of each microstrip antenna is 0.01 wavelengths, the relative permittivity of the dielectric is 2, the dielectric loss tangent is 0.001, and the conductivity is 2.9 Mohm/wavelength.

All elements conform to a paraboloidal surface, with each element tangential to the surface at its center. The equation of a paraboloid is given by:

$$x^2 + y^2 = 4 f z, \qquad (8)$$

where f is the focus of the paraboloid, and x, y, and z are the coordinates of the elements at their centers. The x and y coordinate axes are oriented as shown in Figure 3.1, and the z axis is perpendicular to the x and y axes. We assume that the focal length to diameter ratio (F/D) is 0.4, which makes the focal length 1.35 wavelengths. Since the x and y coordinates of each element are determined by the interelement spacings and the hexagonal configuration described above, we can calculate the z coordinate of each element using equation (8).

Each element is tangential to the paraboloidal surface at its center, and the azimuth (φ) and elevation (θ) angles describing the orientation of each element can be shown to be:

φ = 180 + Arctan(Abs(y/x)) .....Quadrant 1 (defined by + x and + y axes)
270 + Arctan(Abs(x/y)).....Quadrant 2 (defined by - x and + y axes)

Arctan(Abs(y/x))..... Quadrant 3 (defined by –x and –y axes)
90 + Arctan(Abs(x/y))..... Quadrant 4 (defined by +x and –y axes)

$$\theta = \text{Arctan}((\text{sqrt}(x^2+y^2))/(f-z)) / 2 \qquad (9)$$

where x, y, z, and f are as described above and in Figure 3.1. We may define a local z axis at the center of each element, as distinct from the main z axis perpendicular to the central element in the array. θ is then the tilt angle that the local z axis makes with the main z axis, and φ is the rotation of the local z axis with respect to the main z axis.

All simulations were conducted implementing the above equations in the Phased Array Program, "ARRAY".

Chapter 4. Paraboloidal Array Performance: General Discussion

4.1 Assessment of Array Performance

The physical configuration of the array and the characteristics of the microstrip antenna elements have been discussed above. Before presenting the results of the simulation of the antenna, it is instructive to analyze the antenna, at least qualitatively, from a theoretical standpoint to provide a better understanding of its anticipated benefits and applications. We can study the performance of the antenna on the basis of parameters such as gain, side-lobe level, efficiency and polarization dependence, scanning behavior, and mutual coupling. What follows is a brief discussion of each of these factors in the context of the array; a more detailed analysis of some of these factors, such as scanning characteristics and mutual coupling effects, will be furnished later in this thesis.

Gain: A circular aperture antenna of diameter 3.375 wavelengths with 100 % aperture efficiency would have a directivity of 20.5 dB, as can be calculated using the formula $D = 4\pi A/\lambda^2$. We can get a sense of the expected paraboloidal array gain by first considering the gain of a planar, hexagonal array inscribed within the circular aperture. The area of a hexagonal aperture inscribed within such a circular aperture can be shown to be 0.82 dB less than the circular aperture, so that the expected directivity of a planar, hexagonal aperture antenna with 100 % aperture efficiency is 20.5-0.82 = 19.7 dB.

But in the case of a planar, hexagonal array, the aperture size that we get by circumscribing the outermost elements by a hexagon is, in fact, an underestimate of the true array size. Due to the spacings between the planar array elements and the hexagonal array shape, each element in the hexagonal array can be considered to have around it an equivalent array factor aperture area or "cell" defined by a hexagon. The aperture area resulting from the array factor for a planar hexagonal array would thus have a boundary defined by the hexagonal areas encompassing the outermost elements, and not by the edges of the elements themselves. The aperture area of the planar hexagonal array is illustrated in Figure 4.1; at the center of each hexagon in the figure is a circular microstrip patch.

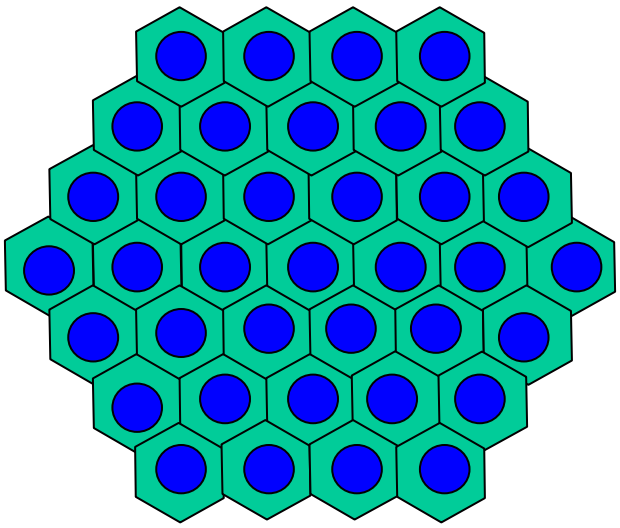

Figure 4.1. Equivalent Aperture Area of Planar Hexagonal Microstrip Array

The equivalent planar array area is consequently closer to the area of a circle circumscribing the array elements. The 100 % efficient directivity of the planar array should thus be higher than 19.7 dB, but a little lower than the circular aperture directivity of 20.5 dB.

In the case of the paraboloidal array, however, the array elements have various inclinations, and we consequently expect the directivity (and gain) of the array to be less than that of the planar array; this is discussed further in the section on "efficiency" below.

Side-lobe Level: A uniformly illuminated rectangular aperture can be shown to have a side-lobe level of -13 dB relative to the maximum. Likewise, a uniformly illuminated circular aperture has a lower side-lobe level of -17.6 dB. Since the array under consideration is neither rectangular nor circular, but is hexagonal, we would expect a side lobe level somewhere between -13 dB and -17.6 dB for broadside scans. Of course, the side lobe level of the array would increase with scan angle.

In a typical circular paraboloidal reflector antenna, the side-lobe level might be greater than -17.6 dB, due to the blockage that occurs from the presence of the subreflector or feed, which increases the side lobes and decreases the gain. However, our array does not suffer from this increase in side-lobe level.

Efficiency: In a conventional reflector antenna, efficiency is typically reduced to about 0.60 due to spillover loss, blockage of the radiation by the subreflector or feed, and other factors. The paraboloidal array has the advantage of not suffering from spillover loss or radiation blockage; however, there are other factors which reduce the antenna efficiency. Specifically, there are two important factors: the vertical inclination of the microstrip antenna elements and the gain-loss due to element polarization mismatch when linear polarization is used.

The vertical inclination of each element in the array increases with radial distance from the center of the array. Since the elements away from the array center are inclined, they are not all oriented so as to produce a pattern maximum in the same direction in the far field. Note that the overall pattern of an array with similar elements is the product of the element factor and the array factor. However, in the paraboloidal array, the element factors for the elements vary due to the different inclinations of the elements, and pattern multiplication does not apply. For convenience in analyzing the array, though, one can come up with an estimated "average" or representative element factor, using an element that has roughly half the inclination that the edge elements have with respect to the central element, and thereby hypothetically separate the element and array factors. The array factor then has a maximum at broadside when not being scanned, but the "average" element factor is not aligned with the array factor, and the maximum of the element factor is not at broadside. Consequently, the product of the element and array factors at broadside is reduced as compared to the case where all elements have the same broadside angle as the array factor. As a result, the efficiency and the gain of the array are reduced. Furthermore, the reduction in contribution to gain from each inclined element is the Cosine of its elevation angle or inclination, as this is the factor by which the projected area of the element in the broadside direction is reduced.

We now estimate the reduction in gain in the paraboloidal array based on the element inclinations and the array's hexagonal configuration. The outermost ring in the paraboloidal array is comprised of 18 elements, and the remainder of the array has 19 elements, i.e. nearly the same. So we may take the elevation angle of an element in the second ring (counting from the outside) as representative of the "average" inclination, neglecting in this first approximation the varying curvature of the paraboloidal surface

(which would slightly increase the angle). The elevation angles of several elements in the second ring are close to 20 degrees, and we can estimate the gain of the paraboloidal array to differ from that of the planar array by a factor of Cosine 20 degrees, or 0.94, which amounts to -0.27 decibels.

Element polarization mismatch when linear polarization is used can also reduce array efficiency. Each element in the array must be both inclined in the direction of the antenna axis and rotated angularly so as to conform to a paraboloidal shape. If linear polarization is used in each antenna element, the rotation of each element causes the polarization to differ for elements not diagonally placed on the array. This misalignment of element polarizations causes a reduction in gain and efficiency. However, this effect can be overcome by noting that if we choose to use circular polarization on the elements instead, then rotation of the elements will have no effect on the polarization of the antenna elements, since circular polarizations are rotationally symmetric. By implementing a circular microstrip patch antenna with a single probe feed and a single slot, we can generate circular polarization.

Overall, assuming implementation of circular polarization, the only factor degrading efficiency is the vertical inclination of the elements, and we may estimate the gain of the antenna to be about 0.27 dB less than the gain of an equivalently sized planar array at broadside.

Scanning: As with any phased array, we would expect the gain of the antenna to decrease with scan angle, the side lobe level to increase, and the beamwidth to broaden. This is easily seen when one realizes that at scan angles away from broadside, the projected area of the antenna is progressively reduced, and consequently the gain is reduced as well. Furthermore, we may anticipate that the scan performance of the paraboloidal array will be similar to that of a similarly sized but planar array. We emphasize once more that since the paraboloidal array is comprised of elements with varying orientations, pattern multiplication does not hold; however, as stated earlier, we may still think in terms of array factors and “average” element factors to intuitively grasp the array’s performance. Recall that we stated earlier that the element patterns are offset from the array factor at broadside by a certain angle, depending on the element inclination. All the element factors except for

the one in the center of the array are offset from the array factor at broadside. As the array factor is scanned off broadside, it becomes more aligned with the element factors of some of the elements, but also simultaneously more mis-aligned with the element factors of other elements, due to the curvature of the parabolodal surface. Overall, the paraboloidal array should therefore yield almost the same gain as the planar array with variation in scan angle.

Mutual Coupling: Most array analyses assume an idealized situation where the elements are assumed to have excitations determined solely by the feed network, and where the principle of pattern multiplication holds. In other words, the interaction between elements that occurs in an array is ignored. This interaction, called mutual coupling, changes the current amplitudes and phases on the elements in the array from the idealized case and thereby alters the radiation pattern of the antenna. Pattern multiplication thus provides only an approximation to the actual antenna pattern. Additionally, mutual coupling depends on polarization, scan direction, and frequency. Further discussion of the effects of mutual coupling on the paraboloidal array will be provided later in this thesis.

4.2 Scanning and Phase Quantization: Background and Performance

The defining characteristic of a phased array is that it can be electronically scanned over a range of angles by implementing various phase shifts in the currents that feed adjacent elements. For example, a planar array of microstrip patches has a broadside main beam perpendicular to the antenna plane when the inter-element phase shift is zero, but by implementing an appropriate inter-element phase shift, we can scan the main beam to a desired angle. However, with the scanning ability of a phased array comes the penalty that at scan angles away from broadside, gain is reduced and beamwidth increases.

In a conformal array such as the paraboloidal array under consideration, we would expect the inter-element phase shifts needed to scan to a desired angle to be non-uniform, unlike what we would expect in a planar array. Furthermore, the feed current phases for each element will be different even when the main beam is at broadside, due to the need to compensate for the different distances traveled by the radiation from different elements to the far field. This is illustrated in Figure 4.2.

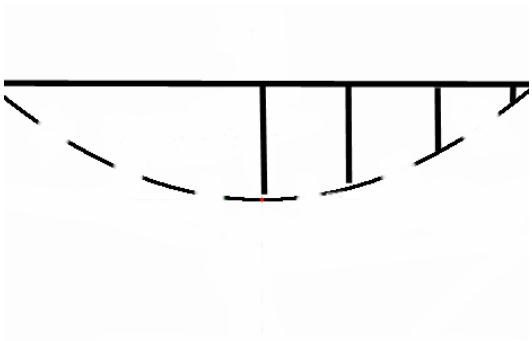

Figure 4.2. Illustration of Distance Differences from Elements to Far Field

From the vertical lines in the diagram, it is clear that the radiation from each element travels different distances to the far field, necessitating phase compensation. Thus, the phase shift required between two elements near the edge of the array would be different from that between two elements at the center, unlike the case of a planar array.

Devices that are commonly integrated into the microstrip line feeding the patches that comprise a phased array include phase shifters and attenuators. A phase shifter typically consists of a switch such as a FET and a length of microstrip line to impart the required phase to the current. Attenuators are used to control the amplitudes of the currents feeding the elements in the array, in case a non-uniform current distribution is required across the antenna aperture. Quantized phase shifters are typically used to feed each element in microstrip arrays. It is impractical and unnecessary to build a phased array with inter-element phase shifts that are exactly what would be needed to produce the desired scanned beam. Typically, the inter-element phase shifts required for scanning are quantized to one of several phase levels, using phase shifters. Such a phase shifter is comprised of a number of phase shifters in series, so as to produce any one of a number of phase shifts for each element. An N-bit phase shifter, reproduced from [7], is shown in Figure 4.3:

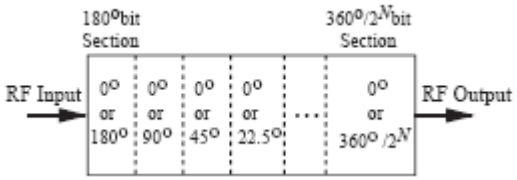

Figure 4.3. N-Bit Phase Shifter

For example, a 5 bit phase shifter consists of 5 phase shifters in series- the first phase shifter imparts a phase shift of 11.25 degrees, the second a phase shift of 22.5 degrees, the third a phase shift of 45 degrees, the fourth a phase shift of 90 degrees, and the last phase shifter imparts a phase shift of 180 degrees. Such a phase shifter can impart any phase shift from 11.25 to 348.75 degrees, in increments of 11.25 degrees. Once the desired phase shifts for the elements in an array so as to scan to a required angle are determined, the quantization levels closest to the desired phase shifts are implemented instead. A quantization error thus results in the process, which typically causes a reduction in gain and an increase in side-lobe levels. We can attempt to improve the scanning performance of the antenna by using a higher-bit quantizer, thereby reducing the quantization error; however, element power loss and cost then increase substantially. Thus, a tradeoff occurs between quantization degradation of the antenna pattern, power efficiency, and cost.

We can thus expect the scanning performance of the paraboloidal array under consideration to vary with scan angle and the quantization level of the phase shifters.

Chapter 5. Simulation Results and Analysis

We now present the scanning and phase quantization simulation results of the paraboloidal array as the scan angle and phase quantization level are varied. First, the scanning simulation results without phase quantization are presented for various scan angles. Then, the scanning simulation results for several levels of phase quantization (5 bit, 4 bit, and 3 bit) are presented. For each paraboloidal array scan pattern presented, the corresponding scan pattern for a planar array is also shown, so as to make clear by comparison the benefits and drawbacks inherent in the use of the paraboloidal array. In all cases where the analysis of the paraboloidal array is done using a pattern multiplication argument, it is implicitly assumed that an "average" element pattern has been defined so that the array factor and element factor can be separated; this, however, is only for illustrative purposes, since pattern multiplication does not strictly hold in the paraboloidal array.

5.1 Scanning: Simulation Results and Analysis

Scanning of the array was done along the plane defined by azimuthal angle $\varphi = 90$ degrees, i.e., scanning was only done as a function of elevation angle θ, with $\theta = 0$ being broadside. The patterns depicted below are $\varphi = 90$ cuts of the overall pattern. Of course, the array can scan to any angle $\varphi = x$ and $\theta = y$, but a $\varphi = 90$ and $\theta = y$ scan suffices to illustrate the performance of the paraboloidal array as compared to a planar one.

It should be noted that scanning beyond a certain angle will not be possible in the paraboloidal array, due to obstruction caused by the curvature of the array. This angle is the elevation angle of the tangent to the elements at the edges of the array. It is related to the inclination or tilt angle θ of the outermost elements as:

$$\text{Maximum Scan Angle} = 90 - \theta \qquad (10)$$

where θ is calculated using equation (9), in which x, y, and z are assumed to describe the location of any element farthest from the center of the array. Since θ is about 29.05 degrees for elements farthest from the array center, the maximum scan angle is 60.95 degrees.

As noted earlier in the thesis, though pattern multiplication does not hold for the paraboloidal array, we may intuitively devise an "average" element factor for the array, with intermediate orientation, such that the product of the resulting "array factor" and the "element factor" gives the overall array pattern. We should also bear in mind that the element factor is considered to be of fixed orientation, in that the element factor does not change with electronic scanning, and that it is only the array factor which is scanned.

In the results shown on the following pages, along with each scan pattern is shown the corresponding far field contour plot. The far field contour plots allow us to assess the full three dimensional pattern of the antennas, rather than just the pattern along a single cut. Each contour plot is analyzed to determine both the highest side lobe level and the first side lobe level. The first side lobe is the side lobe angularly closest to the main beam. Circular polarization was used in feeding the paraboloidal array elements to maximize gain. It was found that when linear polarization was used during simulation, the resultant gains were about 3 dB less than they were when circular polarization was used. This phenomenon was anticipated earlier in this thesis, where it was mentioned that the azimuthal rotation (or rotation in the φ direction) of the elements in the paraboloidal array would change the relative polarizations of the elements if linear polarization were used, thereby decreasing gain. No such polarization misalignment occurs when circular polarization is used in all elements, and the array thus has a higher gain.

In all the pattern plots that follow, the vertical axis (relative gain) ranges from 0 to -50 dB, and the horizontal axis (elevation angle theta) from 0 to 90 degrees.

Figure 5.1 shows the broadside pattern of the paraboloidal array, followed by the corresponding contour plot.

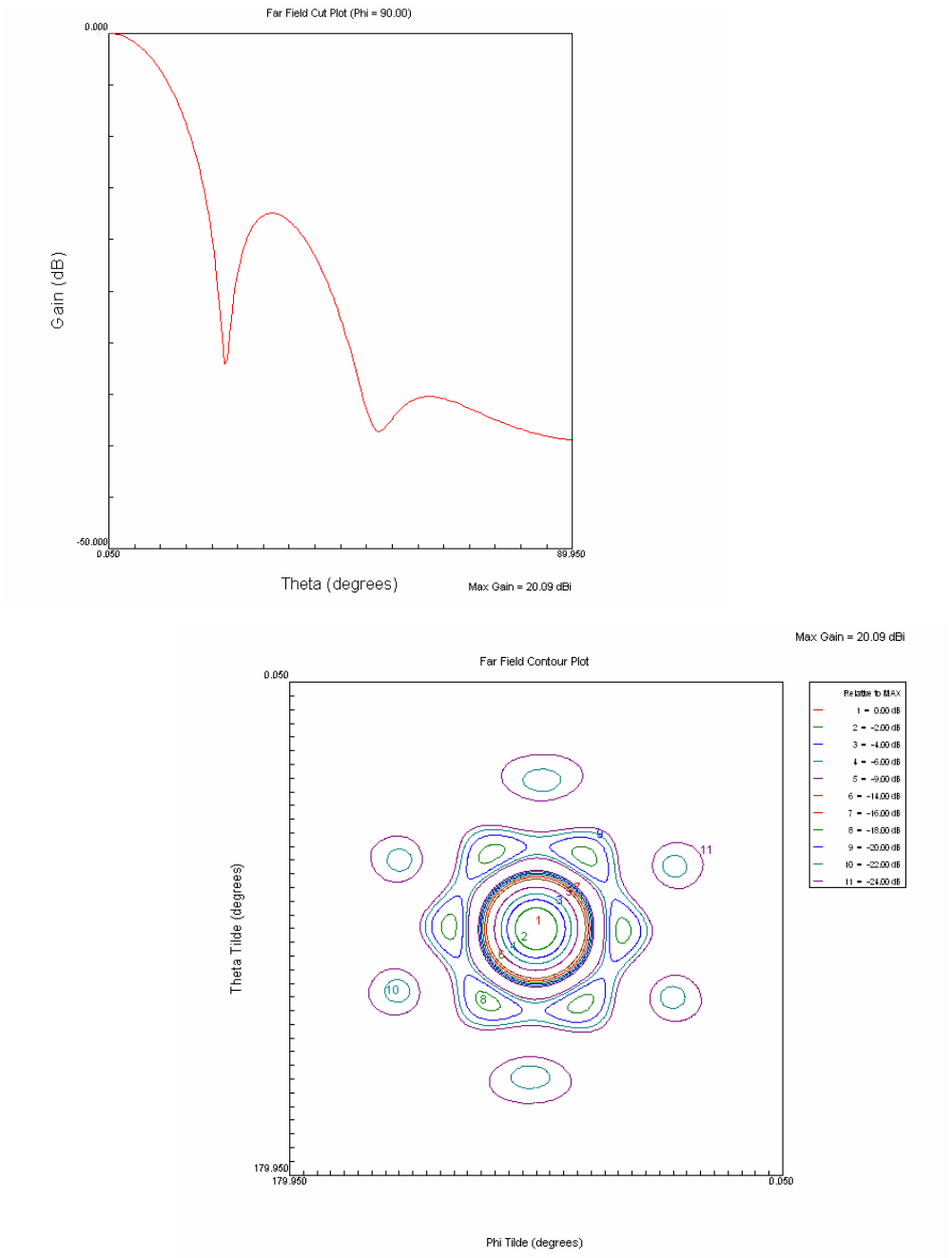

Figure 5.1. Broadside Pattern and Contour Plot for Paraboloidal Array: The gain of the array is 20.09 dB, and the first (and highest SLL) is -18 dB.

The corresponding plots of the planar array are shown in Figure 5.2.

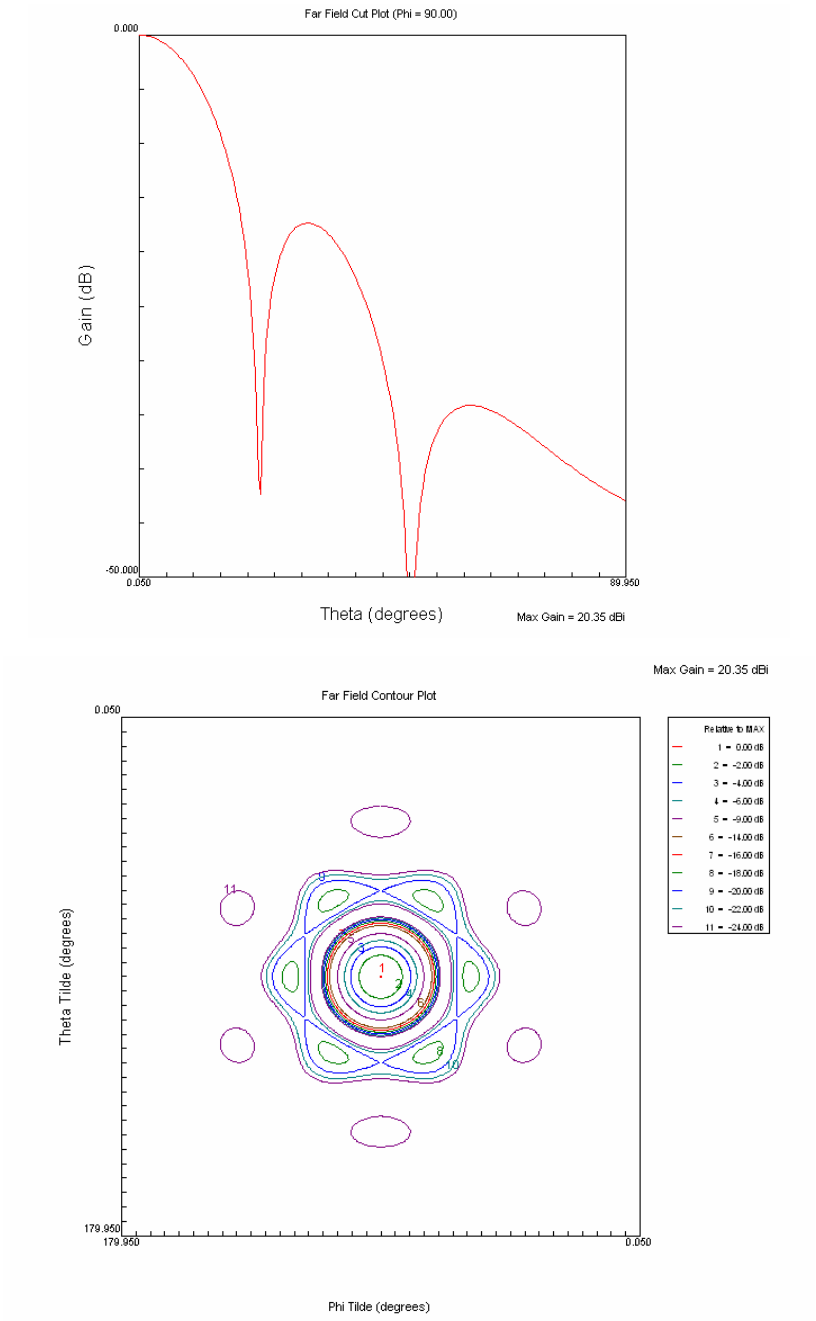

Figure 5.2. Broadside Pattern and Contour Plot for Planar Array: The gain of the planar array is 20.35 dB and the first (and highest) SLL is -18 dB.

The gain of 20.35 dB validates the discussion on the equivalent planar array aperture area earlier in this thesis, in that it is within the estimated range.

The planar array thus yields 0.26 dB more gain than the paraboloidal array. This is because all the elements except the central one in the paraboloidal array are inclined at an angle with respect to the z axis, where the z axis is perpendicular to the central element. The maximums of the patterns of each of the elements are thus not aligned with the array factor maximum, as was anticipated earlier in this thesis, and this causes a slight reduction in gain. The gain loss of 0.26 dB of the paraboloidal array relative to the planar array is almost exactly the gain loss anticipated earlier (0.27 dB).

Figure 5.3 is the pattern of the paraboloidal array when it is scanned 15 degrees, followed by the corresponding contour plot.

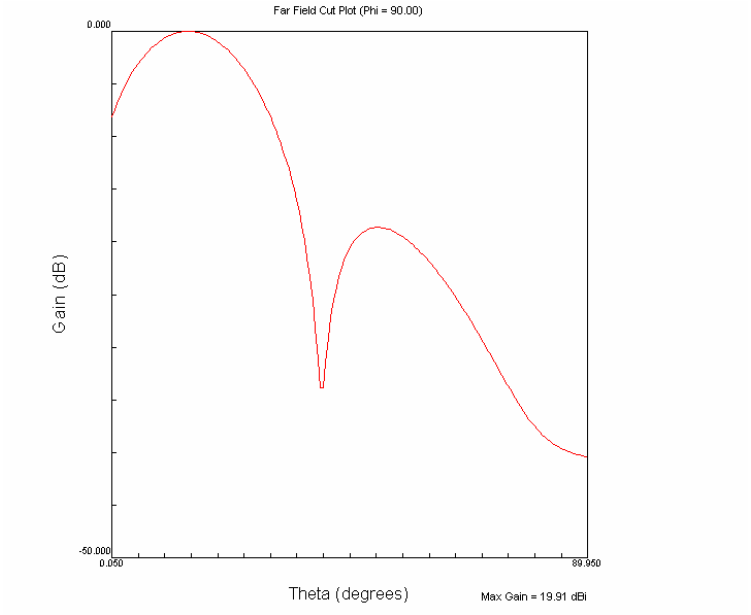

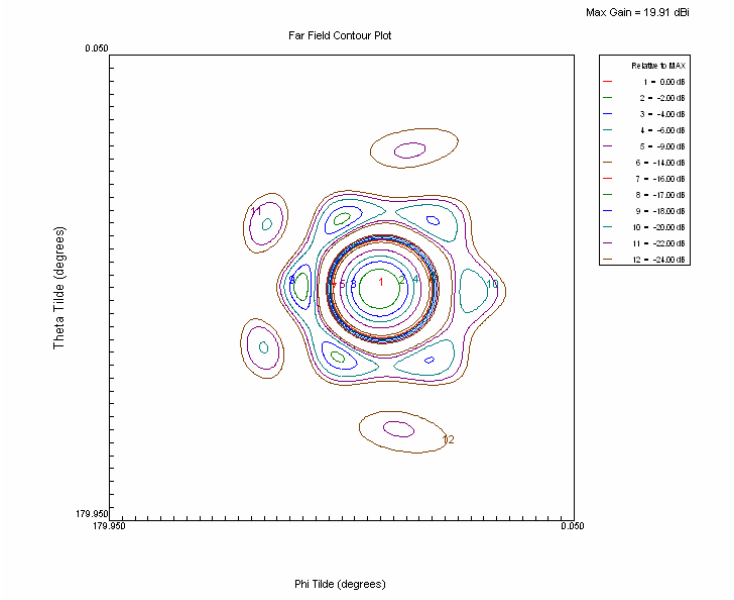

Figure 5.3. 15 Deg Scan Pattern and Contour Plot for Paraboloidal Array

The gain of the array has decreased slightly, from 20.09 dB broadside to 19.91 dB, a change of 0.18 dB. Additionally, the SLL is now -17 dB. Next, the corresponding plots for the planar array are shown.

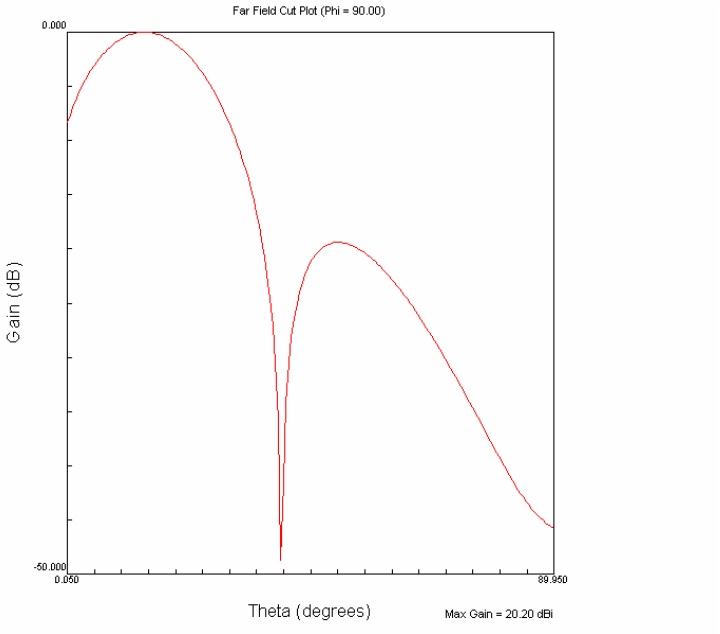

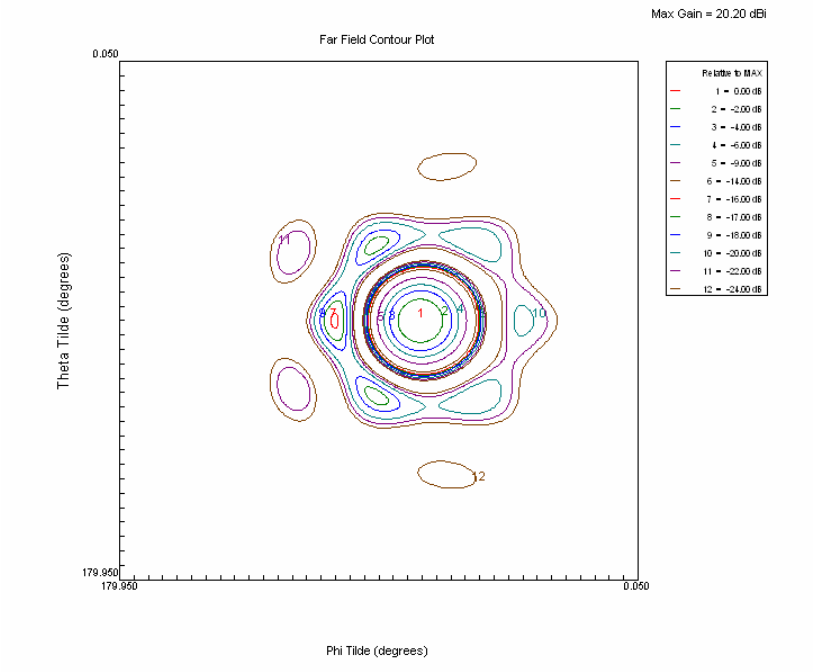

Figure 5.4. 15 Deg Scan Pattern and Contour Plot for Planar Array

It is seen that the planar array gain decreases from 20.35 dB to 20.20 dB, a change of 0.15 dB. The first (and highest) SLL is -16 dB. Scanning further to angles of 30 degrees and 45 degrees reinforces the trend of similar gain losses in the two arrays. The scan patterns and contour plots of the paraboloidal and planar arrays for these scan angles are shown successively in Figures 5.5-5.8 for comparison.

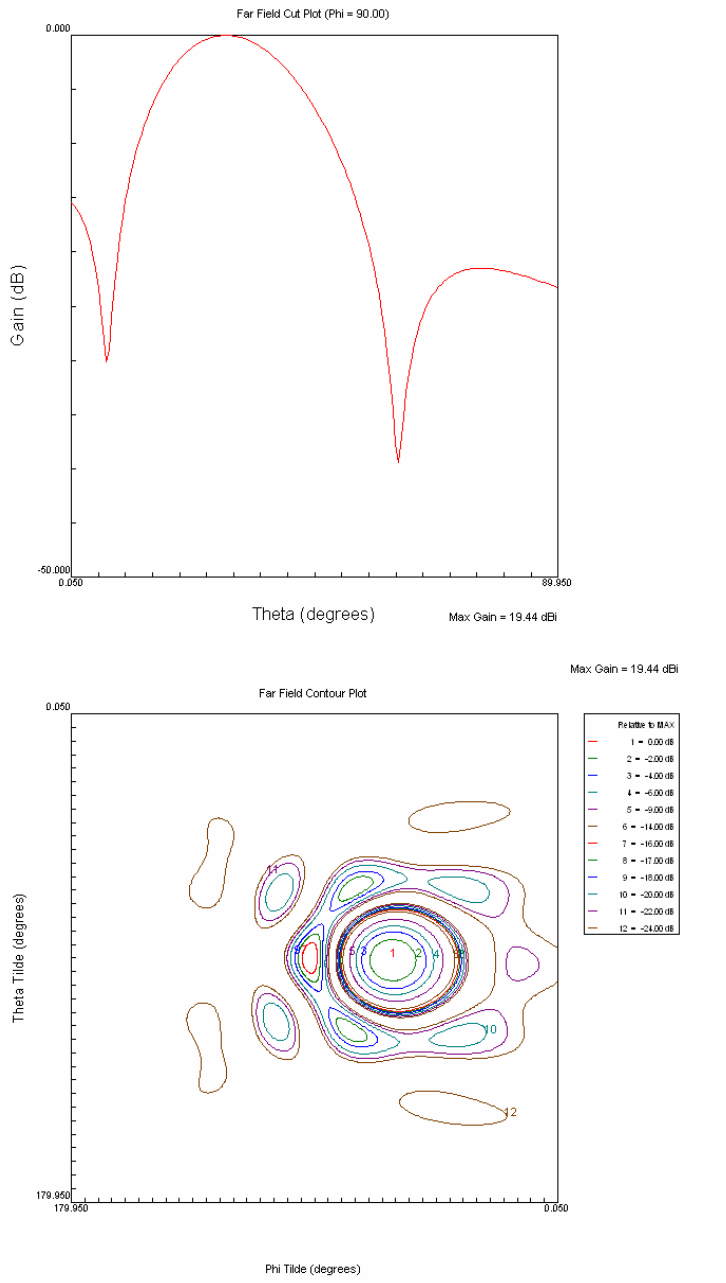

Figure 5.5. 30 Deg Scan Pattern and Contour Plot for Paraboloidal Array: The gain is 19.44 dB and the SLL is -16 dB

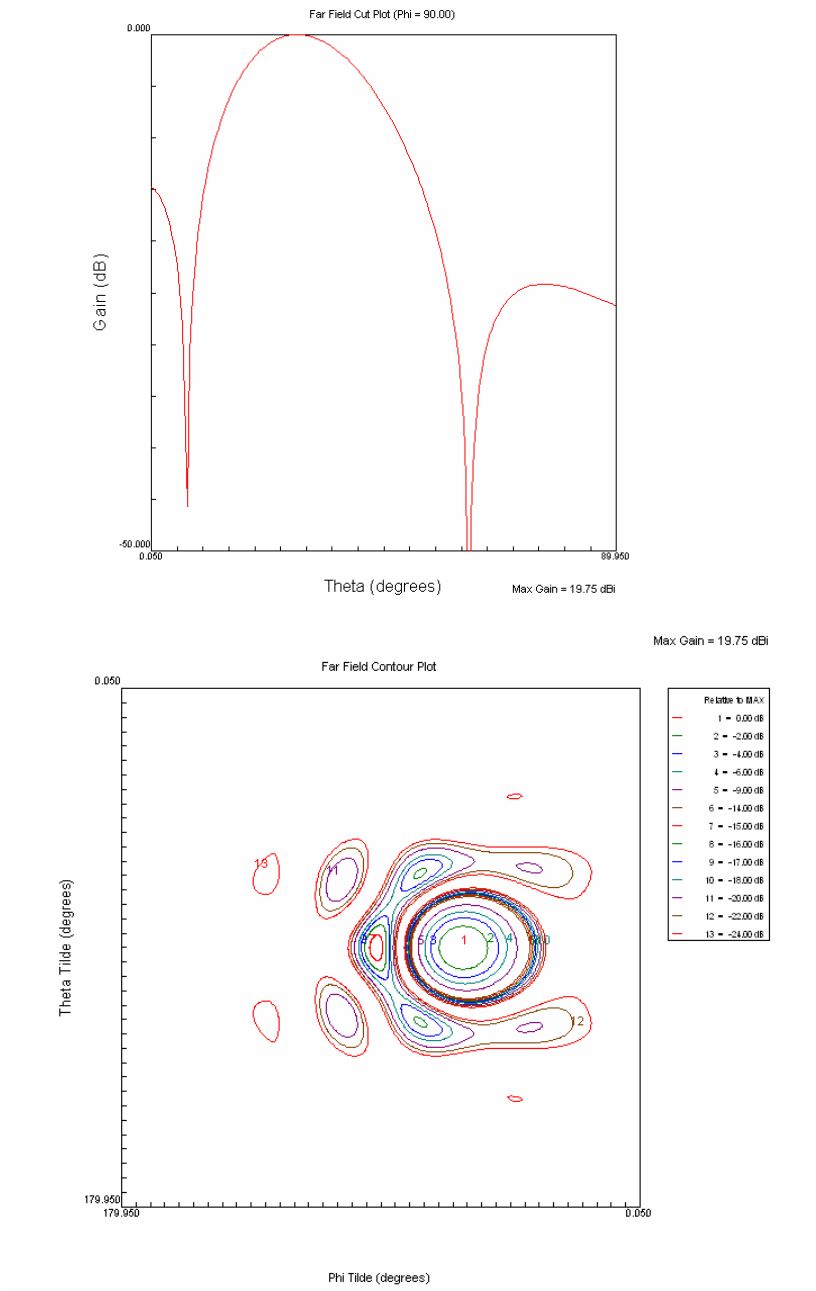

Figure 5.6. 30 Deg Scan Pattern and Contour Plot for Planar Array: The gain is 19.75 dB, and the first (and highest) SLL is -15 dB.

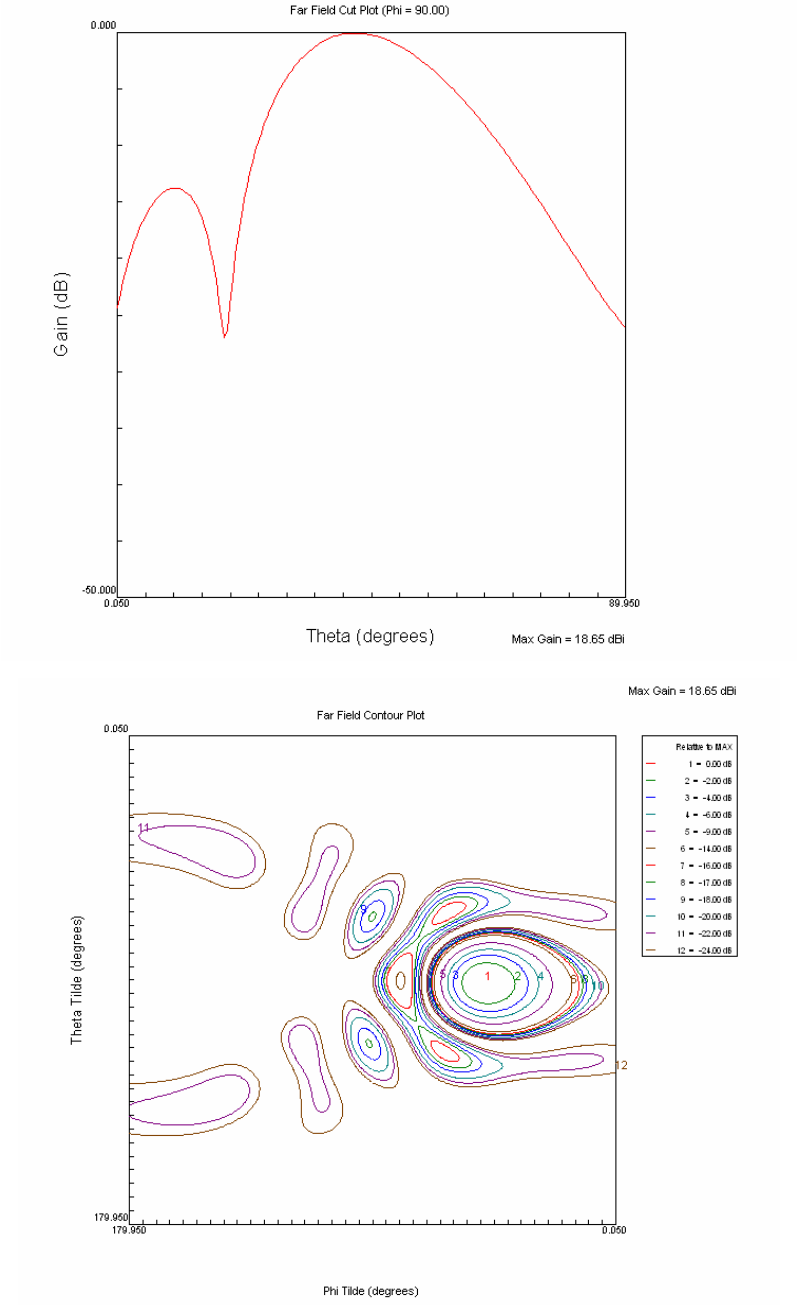

Figure 5.7. 45 Deg Scan Pattern and Contour Plot for Paraboloidal Array: The gain is 18.65 dB and the SLL is -14 dB.

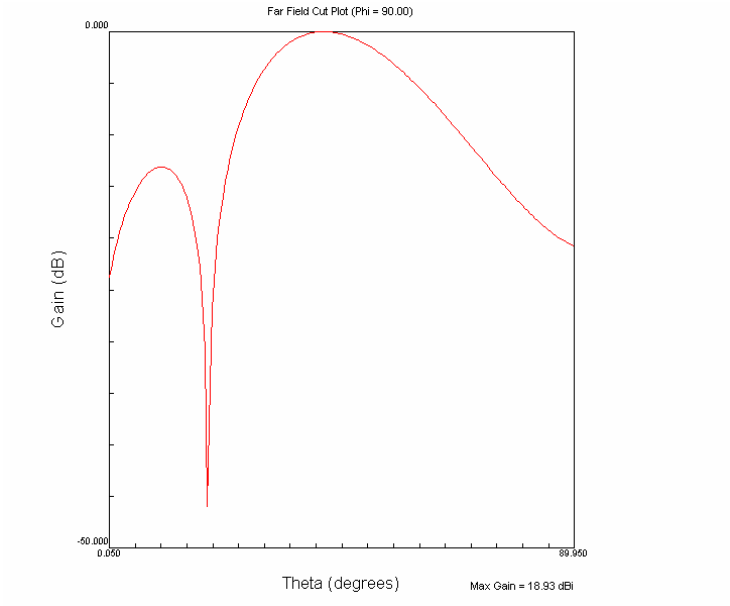

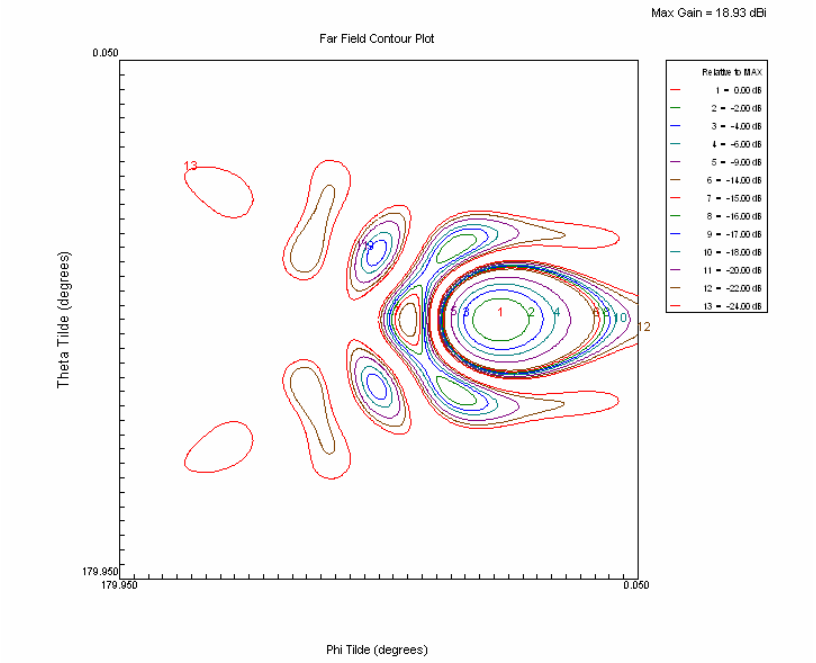

Figure 5.8. 45 Deg Scan Pattern and Contour Plot for Planar Array: The gain is 18.93 dB, the first (and highest) SLL is -14 dB.

As seen above, for scan angles of 15 degrees, 30 degrees, and 45 degrees, the planar array suffers gain-losses of about 0.2 dB, 0.6 dB, and 1.4 dB relative to the broadside gain. The paraboloidal array suffers corresponding almost identical gain-losses of 0.2 dB, 0.7 dB, and 1.4 dB.

We now rationalize the similar gain-losses obtained for the two arrays. When scanned to an angle, the gain (or more specifically, the array factor gain) of a planar array decreases by a factor equal to the cosine of that angle, due to the projected area of the array in the direction of scanning decreasing by that factor. The cosines of 15 degrees, 30 degrees, and 45 degrees give factors of 0.966, 0.866, and 0.707, respectively. These factors correspond to losses in decibels of 0.2 dB, 0.6 dB, and 1.5 dB. It is seen that there is excellent agreement between the gain losses predicted by the decreased array factor and the planar and paraboloidal array results obtained above. The curvature of the paraboloidal surface causes an increased alignment of the main lobes of some of the element patterns with the array factor (which compensates, to an extent, for the decrease in array gain with scanning), but simultaneously, an increased mis-alignment of element patterns and the array factor for elements on the opposite side of the center. The result of these two effects is that the scanning gain loss of the paraboloidal array is almost identical to that of the planar array.

A discrepancy is noted in the scanned beams- careful examination of the patterns reveals that the arrays do not scan precisely to the angle specified by the array factor, but rather to slightly smaller angles. For smaller scan angles, the difference between the two is not substantial, but as the scan angles are increased, the array does not scan to the angle specified in the array factor, but to significantly lower angles. For example, when the array factor is scanned to 15 degrees, the planar array pattern has a peak at approximately 15 degrees; however, the planar array pattern peaks for array factor scans to 30 degrees, 45 degrees, 60 degrees, and 75 degrees occur at 28.3 degrees, 41.7 degrees, 53 degrees, and 61 degrees. When the paraboloidal array is scanned to 45 degrees, the array pattern peak occurs at 42.5 degrees. This discrepancy, as well as the slight difference between predicted and simulated scan gains for the arrays, is easily explained when it is remembered that the overall pattern of the array is the product of the array factor and the element pattern. Though the array factor has a peak at the desired scan angle, the element pattern has a peak

at broadside (in the planar array), and the product of the two factors may thus have a peak at an angle other than broadside. Additionally, the gain of the array at a scan angle may be different from what is predicted based on the reduced projected array area (or reduced array factor) alone, due to the influence of the element patterns. The element pattern in the case of the planar array is the pattern of a single microstrip patch antenna, which has a peak at broadside.

It is also instructive to study the scanning performance of the arrays with respect to side-lobe level and half-power beamwidth. Examination of the contour plots for the planar array reveals that the first (and highest) side-lobe levels at 0 degrees (broadside), 15 degrees, 30 degrees, and 45 degrees are -18 dB, -16 dB, -15 dB, and -14 dB, respectively. The highest side lobes are located closest to the main beam in the array patterns for both arrays. The paraboloidal array contour plots show that the highest side lobe levels at 0 degrees, 15 degrees, 30 degrees, and 45 degrees are -18 dB, -17 dB, -16 dB, and -14 dB, respectively. Thus, it is seen that the highest side lobe level in both the planar and paraboloidal array patterns steadily increases with scan angle, as we would expect. Furthermore, the rate of increase of side lobe level is about 1 dB per 15 degree increase in scan angle for both arrays.

Examination of the array patterns of the paraboloidal and planar arrays reveals that while their gains differ slightly, their contour plots are very similar. This is to be expected since, in the paraboloidal array, we have simply tilted the elements, but not changed the symmetry or shape of the array in any way relative to the planar array.

Furthermore, we can see from the contour plots that in both paraboloidal and planar arrays, the maxima of the first side lobes occur in the directions at which the vertices of the hexagonal configuration are located- the contour plots maintain a hexagonal symmetry. This is because the dimension of the array is greatest between opposite vertices, and consequently, the first side lobes should occur in those directions.

The half-power beamwidths for the planar array at 0 degrees, 15 degrees, 30 degrees, and 45 degrees are 18.2 degrees, 19 degrees, 20.6 degrees, and 23.7 degrees, respectively. The corresponding beamwidths for the paraboloidal array are 18.3 degrees, 19.2 degrees, 20.6 degrees, and 24 degrees. Both arrays thus show comparable increases in beamwidth with increasing scan angles.

5.2 Phase-Quantized Scanning: Simulation Results and Analysis

This section will present the simulation results obtained when scanning is performed with various levels of phase quantization implemented.

We first present the broadside patterns of the paraboloidal array with different levels of phase quantization. The phase quantizations simulated were 5 bit (quantum is 11.25 degrees), 4 bit (quantum is 22.5 degrees) and 3 bit (quantum is 45 degrees). Of course, the broadside quantized patterns of the planar array are identical to the non-quantized patterns, since there, all interelement phase shifts are 0. The results of phase-quantized scanning are shown in Figures 5.9-5.23.

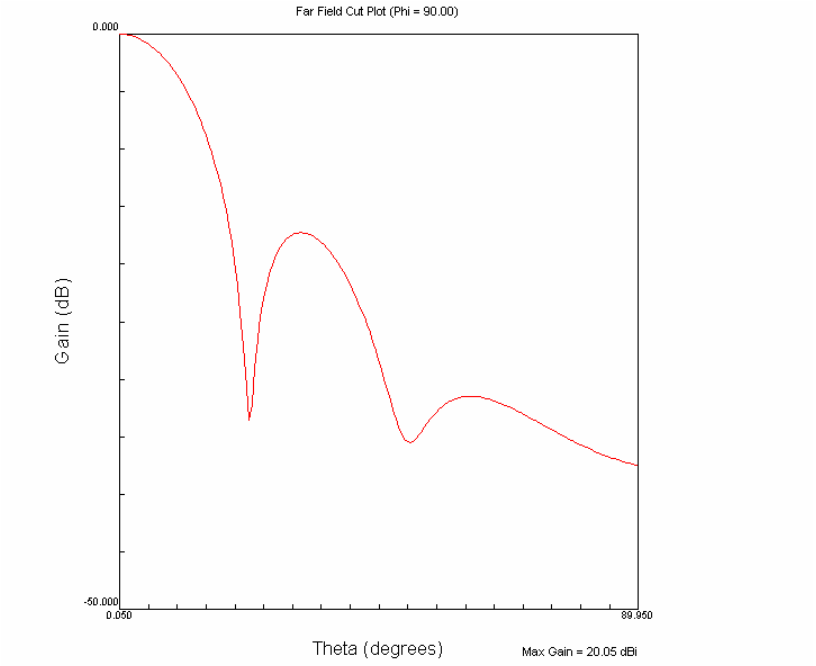

Figure 5.9. Broadside 5 bit Phase-quantized Pattern for Paraboloidal Array

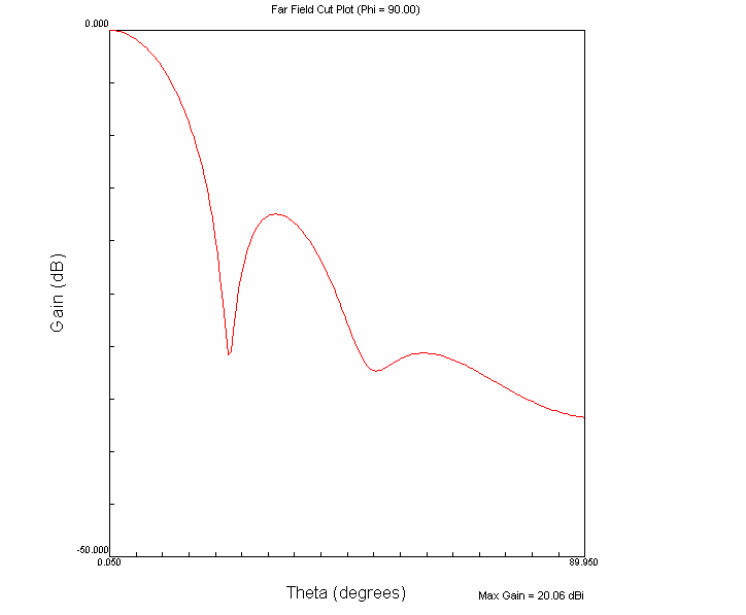

Figure 5.10. Broadside 4 bit Phase-quantized Pattern for Paraboloidal Array

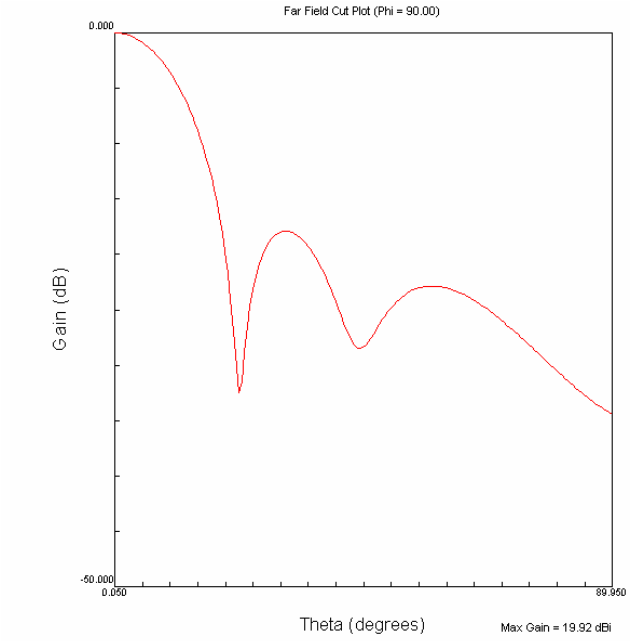

Figure 5.11. Broadside 3 bit Phase-quantized Pattern for Paraboloidal Array

As can be seen in Figures 5.9-5.11, there is not much variation in the gain of the paraboloidal array with 5 and 4 bit quantization when the beam is oriented broadside. With 3 bit quantization, the gain decreases from 20.09 dB to 19.92 dB. The side-lobe level and the half-power beamwidth of the quantized broadside beams remain nearly the same as in the non-quantized case.

Slightly more variation with phase quantization level in the patterns occurs when the beam is scanned away from broadside. Shown in Figures 5.14-5.25 are the scan patterns of the paraboloidal array, along with corresponding patterns of the planar array, for various levels of phase quantization.

With 5 bit phase quantization, neither the paraboloidal array nor the planar array suffers appreciable gain-loss for any scan angle relative to the case where phase quantization is not performed. Furthermore, the side-lobe levels and the half-power beamwidths of the 5 bit-quantized patterns are practically identical to those where phase quantization is not performed. For lower levels of phase quantization, both arrays suffer some minimal performance degradation with scanning. The specific amount of performance degradation suffered by each array relative to the case where phase quantization is not performed is found to be dependent on the scan angle. To illustrate this, the paraboloidal and planar array patterns for selected scan angles for 4 and 3 bit phase quantizations are shown in Figures 5.12-5.23.

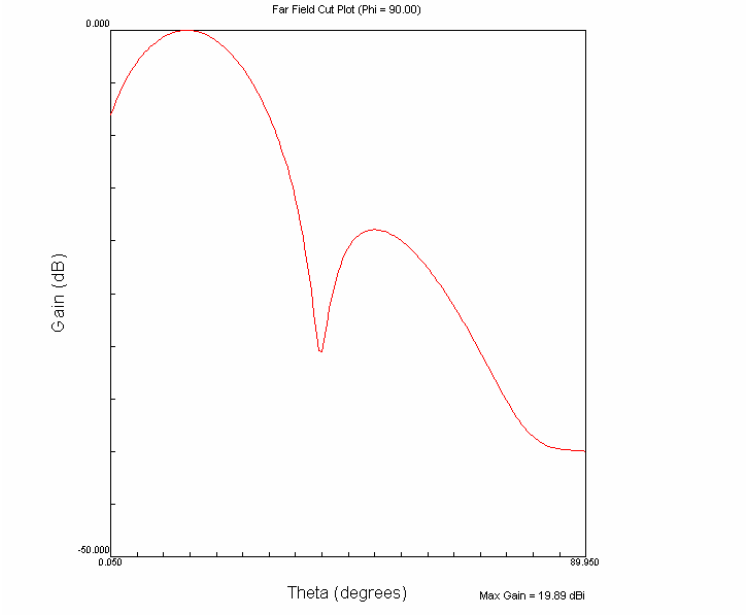

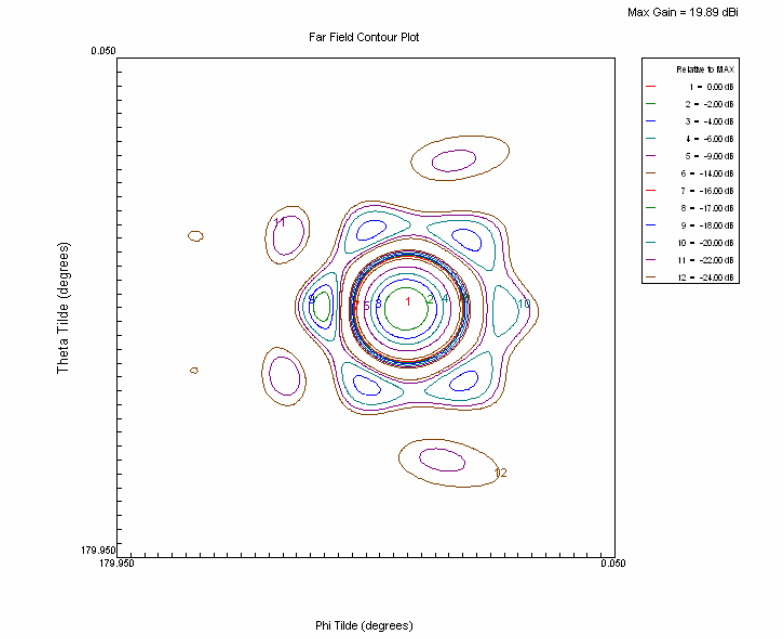

Figure 5.12. 15 deg, 4 bit Phase-quantized Pattern and Contour Plot for Paraboloidal Array: The gain is 19.89 dB, and the first (and highest) SLL is -17 dB.

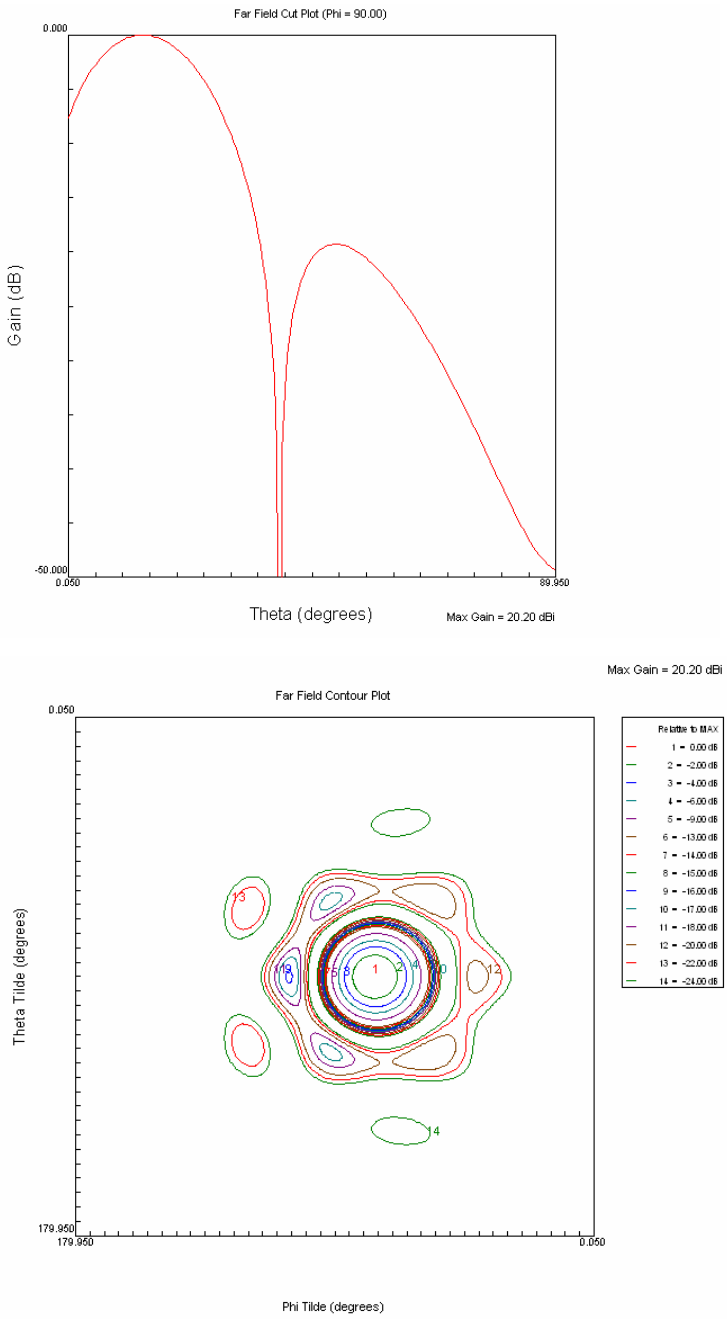

Figure 5.13. 15 deg, 4 bit Phase-quantized Pattern and Contour Plot for Planar Array: The gain is 20.20 dB, and the first (and highest) SLL is -16 dB

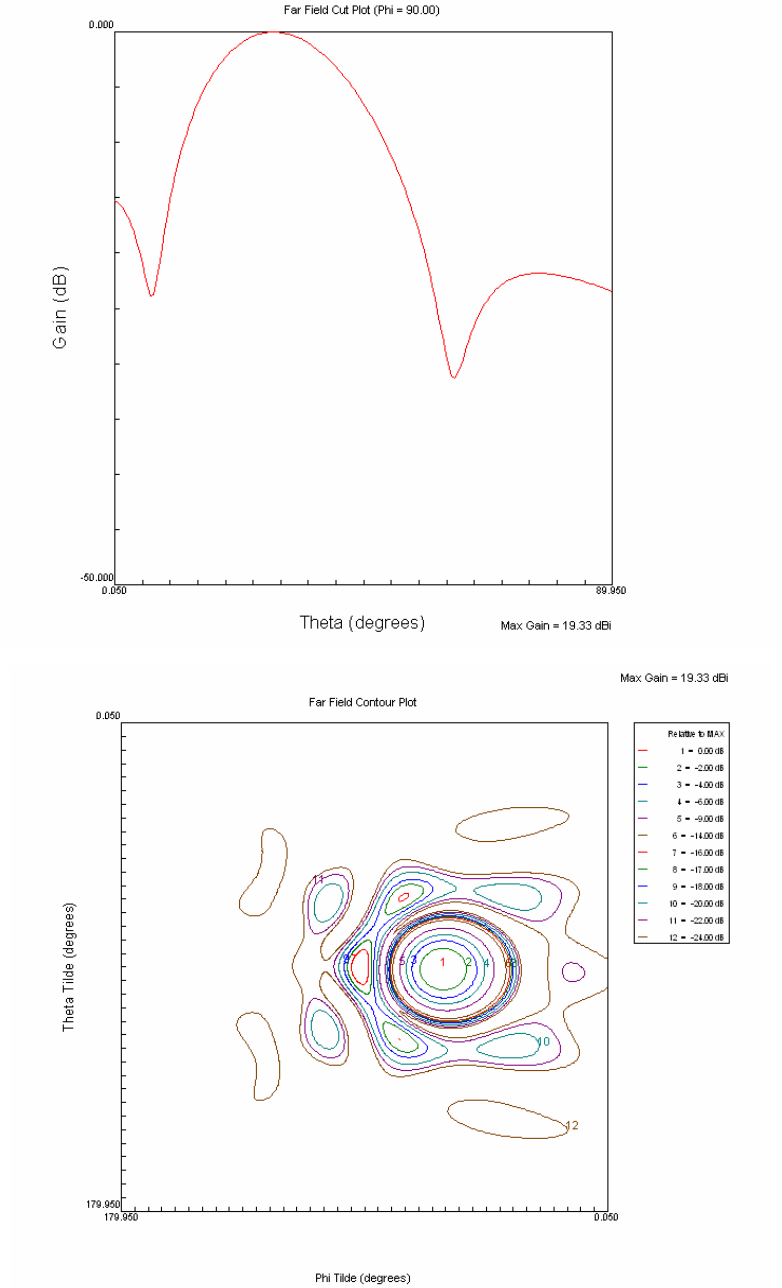

Figure 5.14. 30 Deg, 4 bit Phase-quantized Pattern and Contour Plot for Paraboloidal Array: The gain is 19.33 dB, and the first (and highest) SLL is -16 dB.

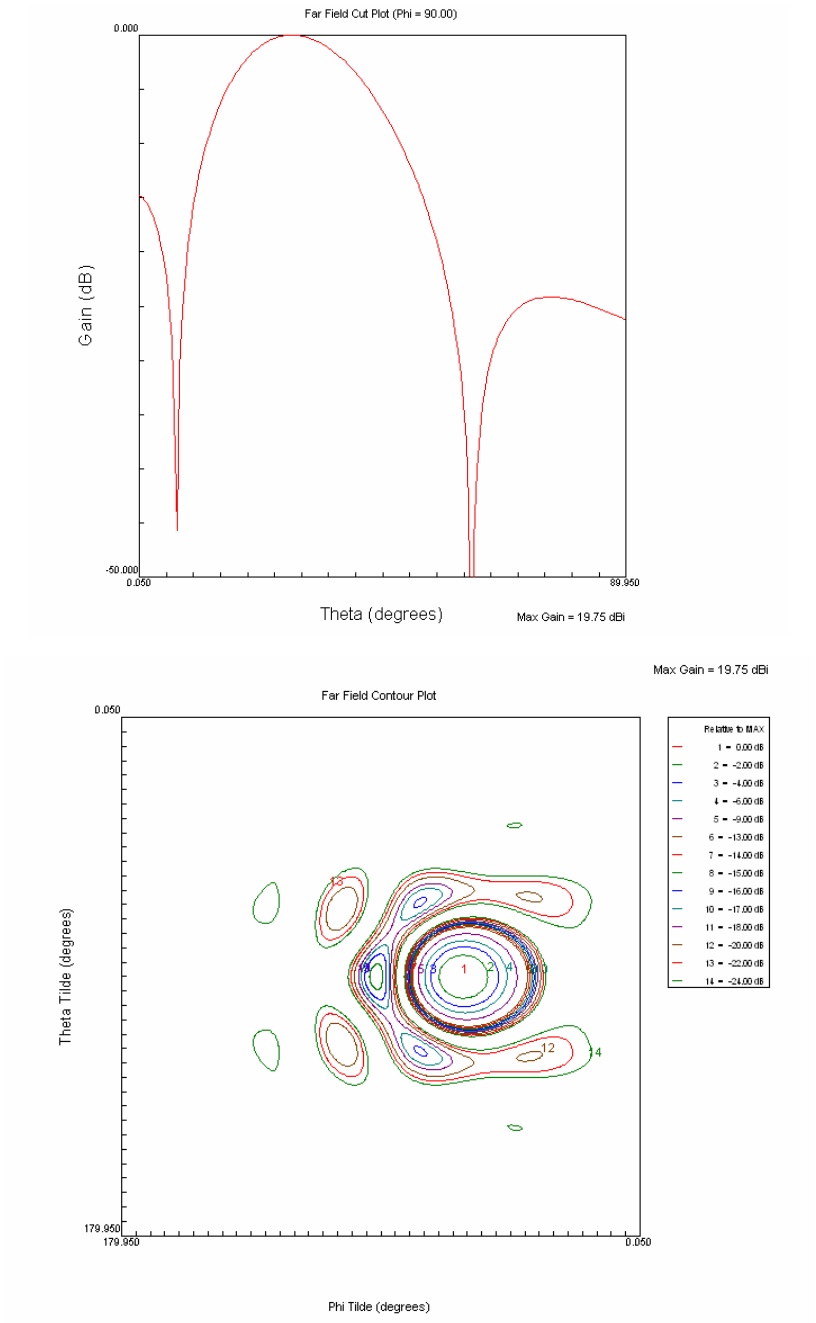

Figure 5.15. 30 Deg, 4 bit Phase-quantized Pattern and Contour Plot for Planar Array: The gain is 19.75 dB, the SLL is -15 dB.

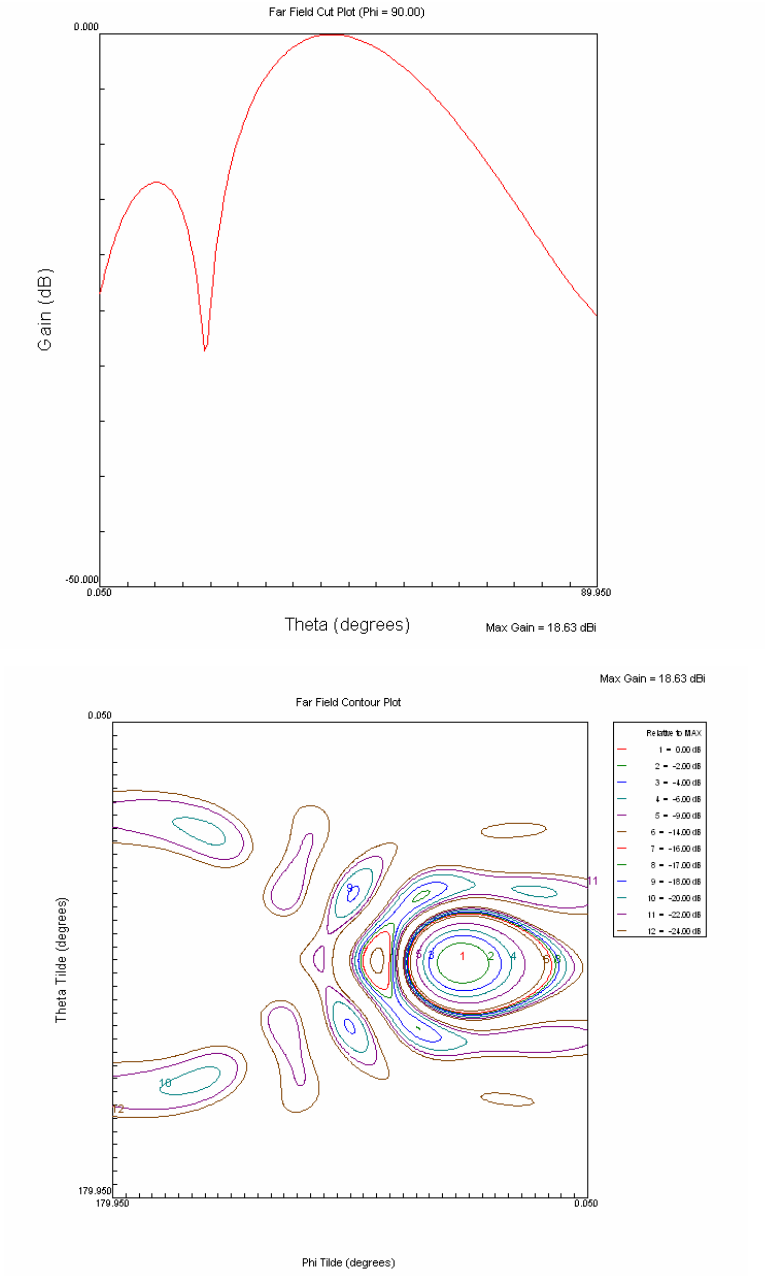

Figure 5.16. 45 Deg, 4 bit Phase-quantized Pattern and Contour Plot for Paraboloidal Array: The gain is 18.63 dB, the SLL is -14 dB.

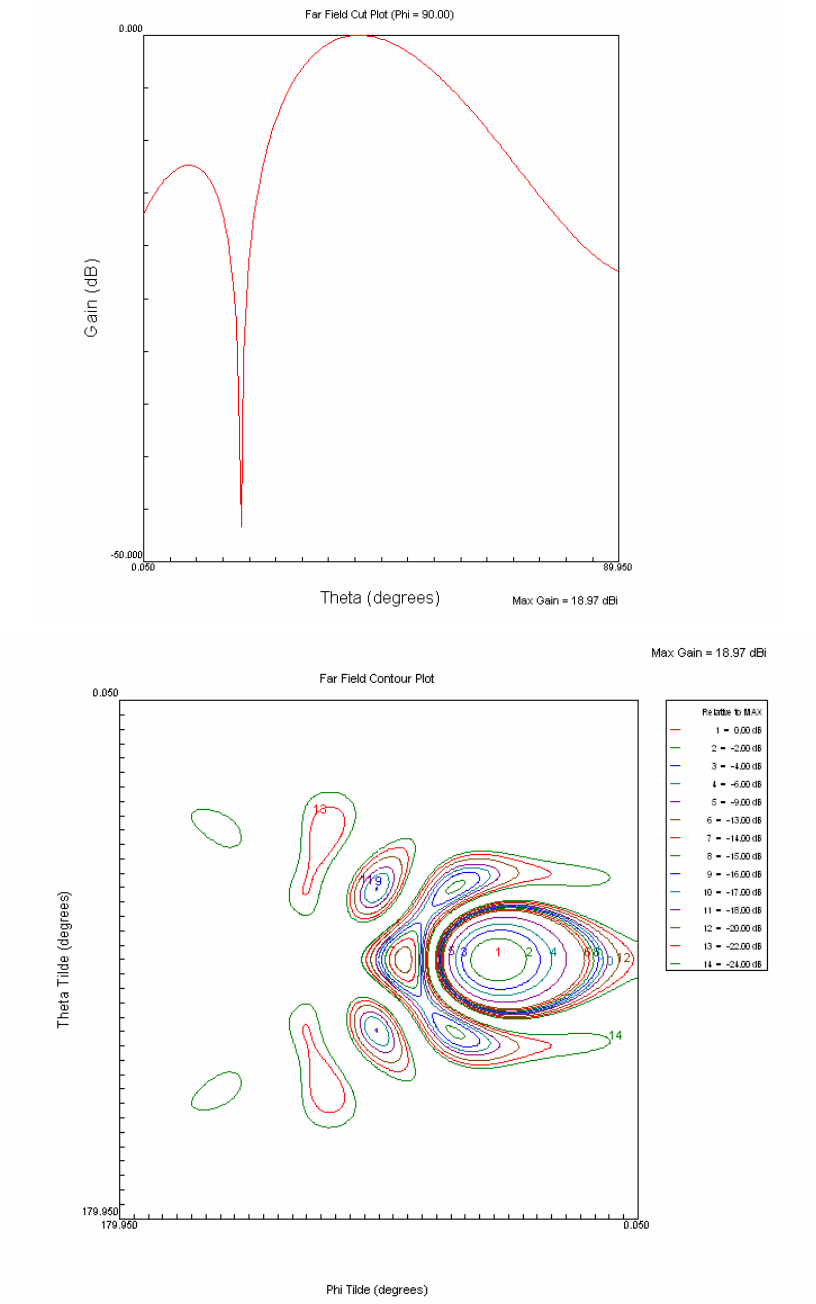

Figure 5.17. 45 Deg, 4 bit Phase-quantized Pattern and Contour Plot for Planar Array: The gain is 18.97 dB, and the first (and highest) SLL is -13 dB.

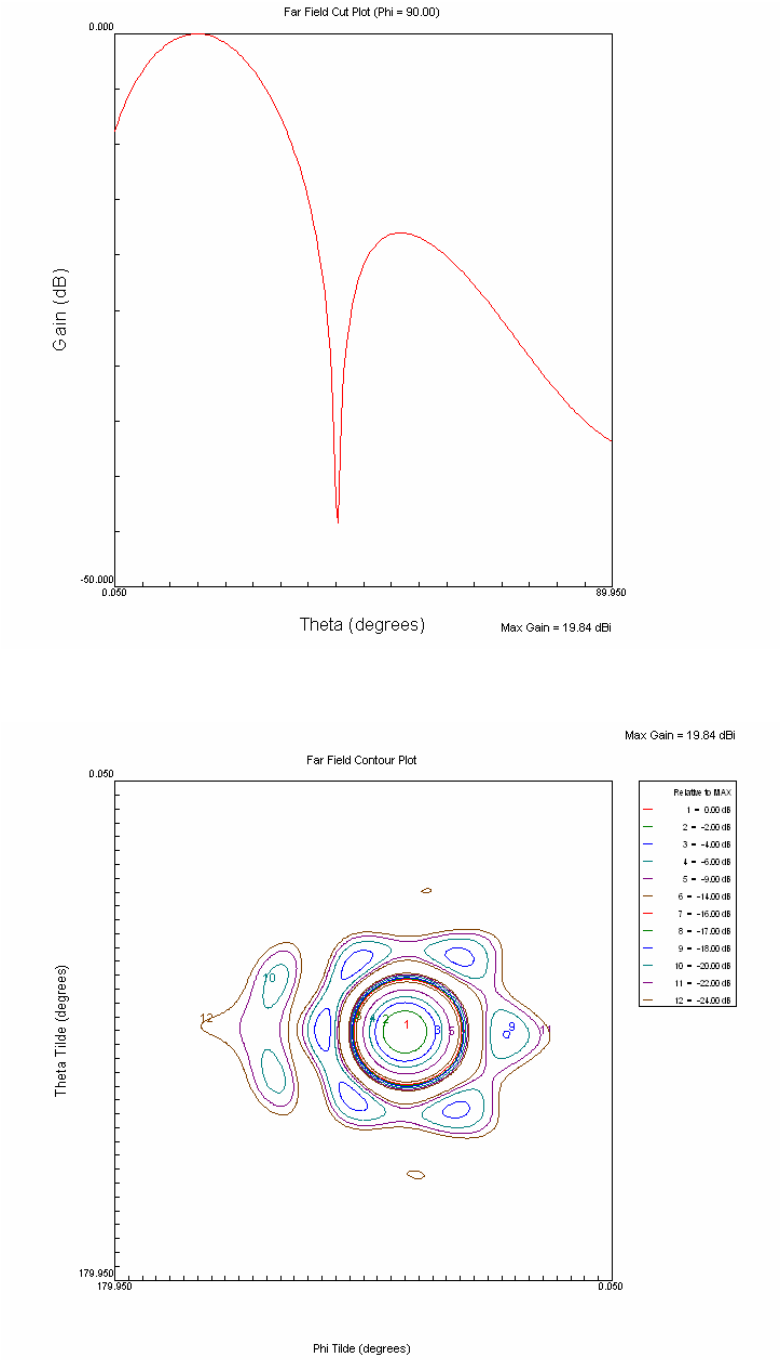

Figure 5.18. 15 Deg, 3 bit Phase-quantized Pattern and Contour Plot for Paraboloidal Array: The gain is 19.84 dB, the SLL is -18 dB.

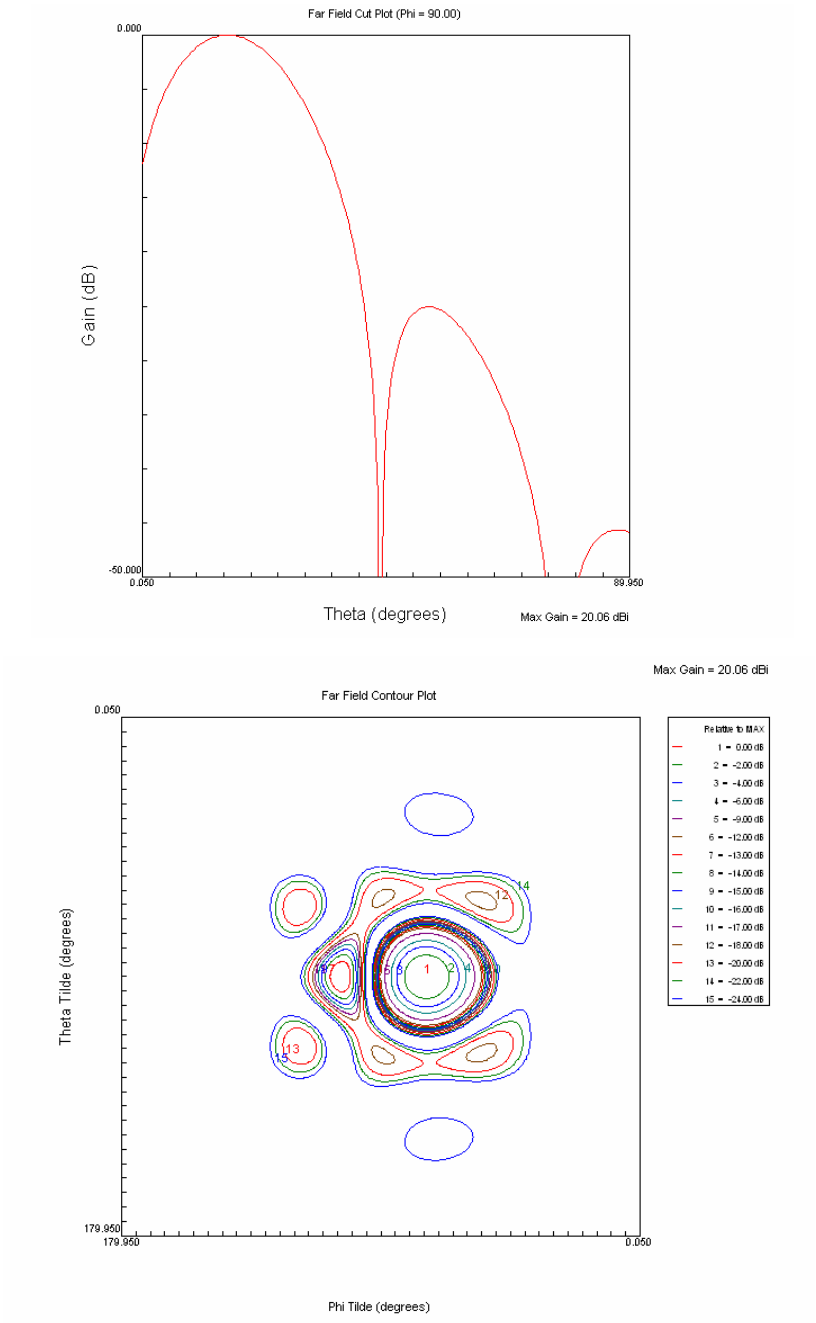

Figure 5.19. 15 Deg, 3 bit Phase-quantized Pattern and Contour Plot for Planar Array: The gain is 20.05 dB, the SLL is -13 dB.

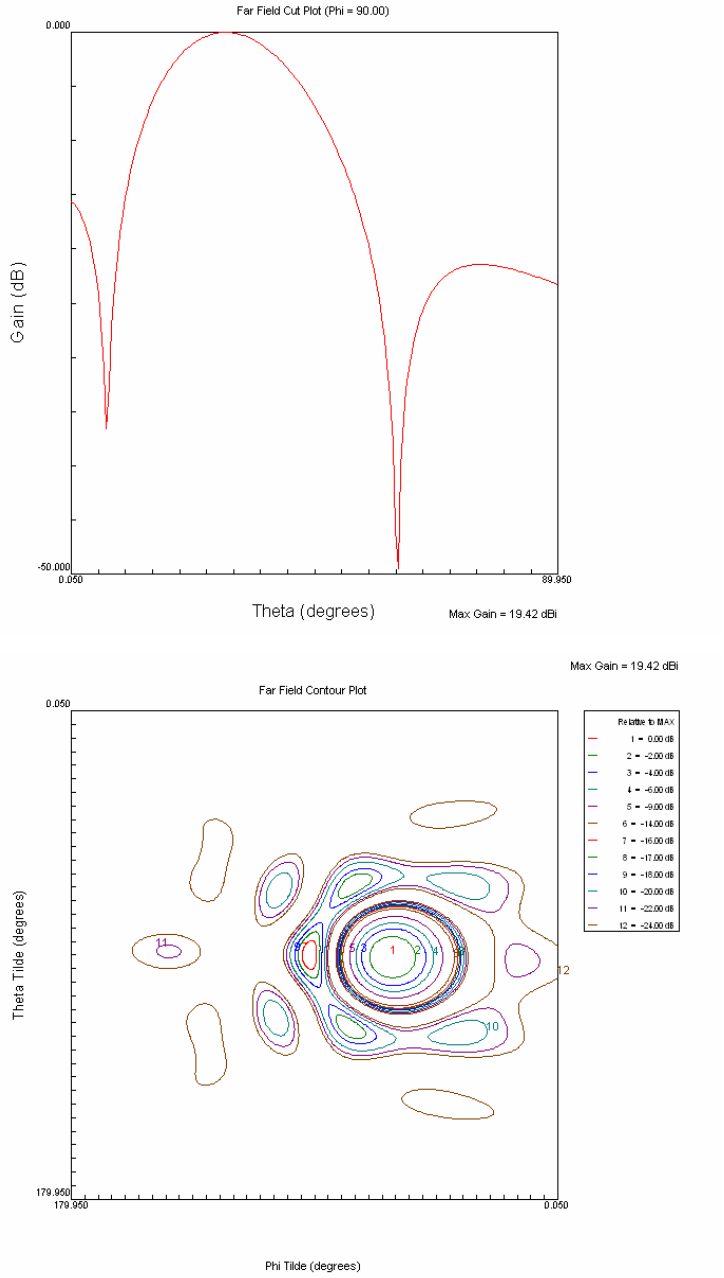

Figure 5.20. 30 Deg, 3 bit Phase-quantized Pattern and Contour Plot for Paraboloidal Array: The gain is 19.42 dB, the SLL is -16 dB.

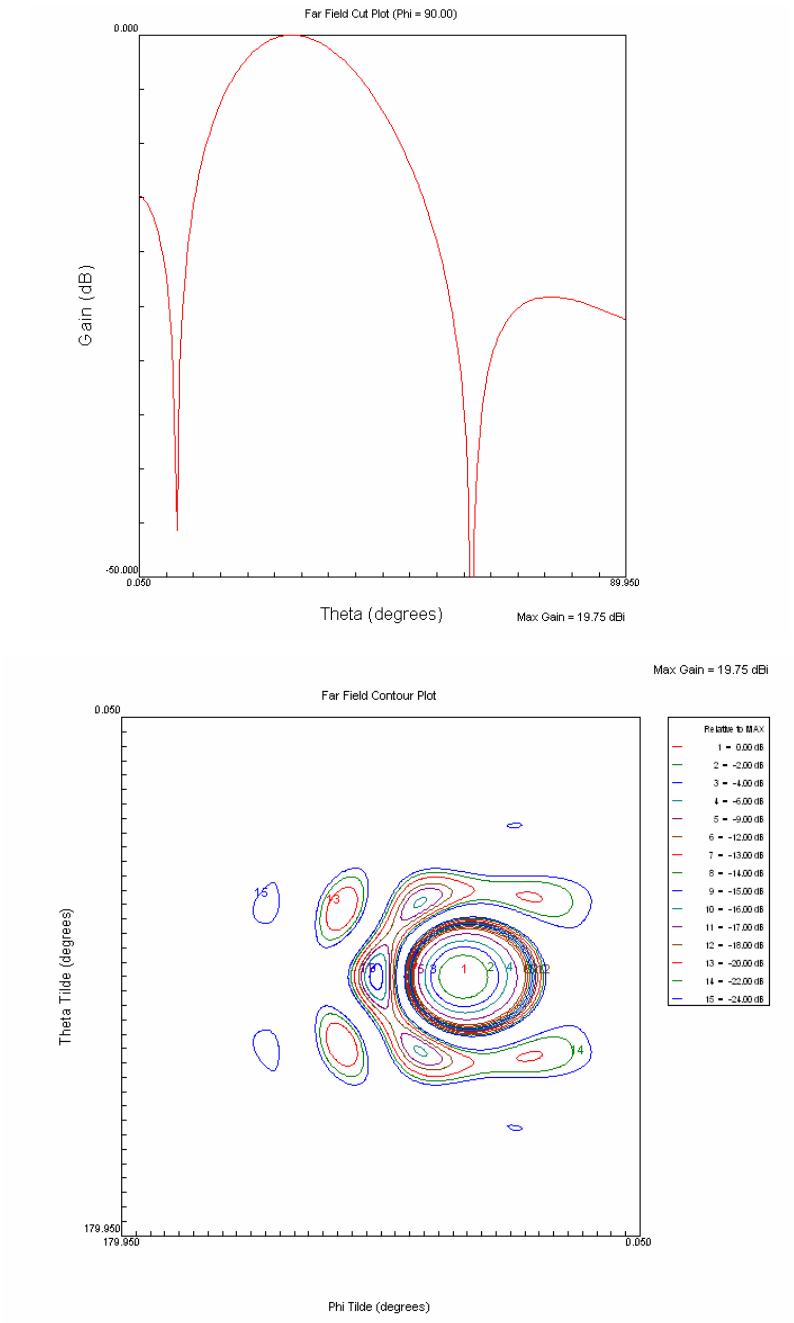

Figure 5.21. 30 Deg, 3 bit Phase-quantized Pattern and Contour Plot for Planar Array: The gain is 19.75 dB, and the first (and highest) SLL is -15 dB.

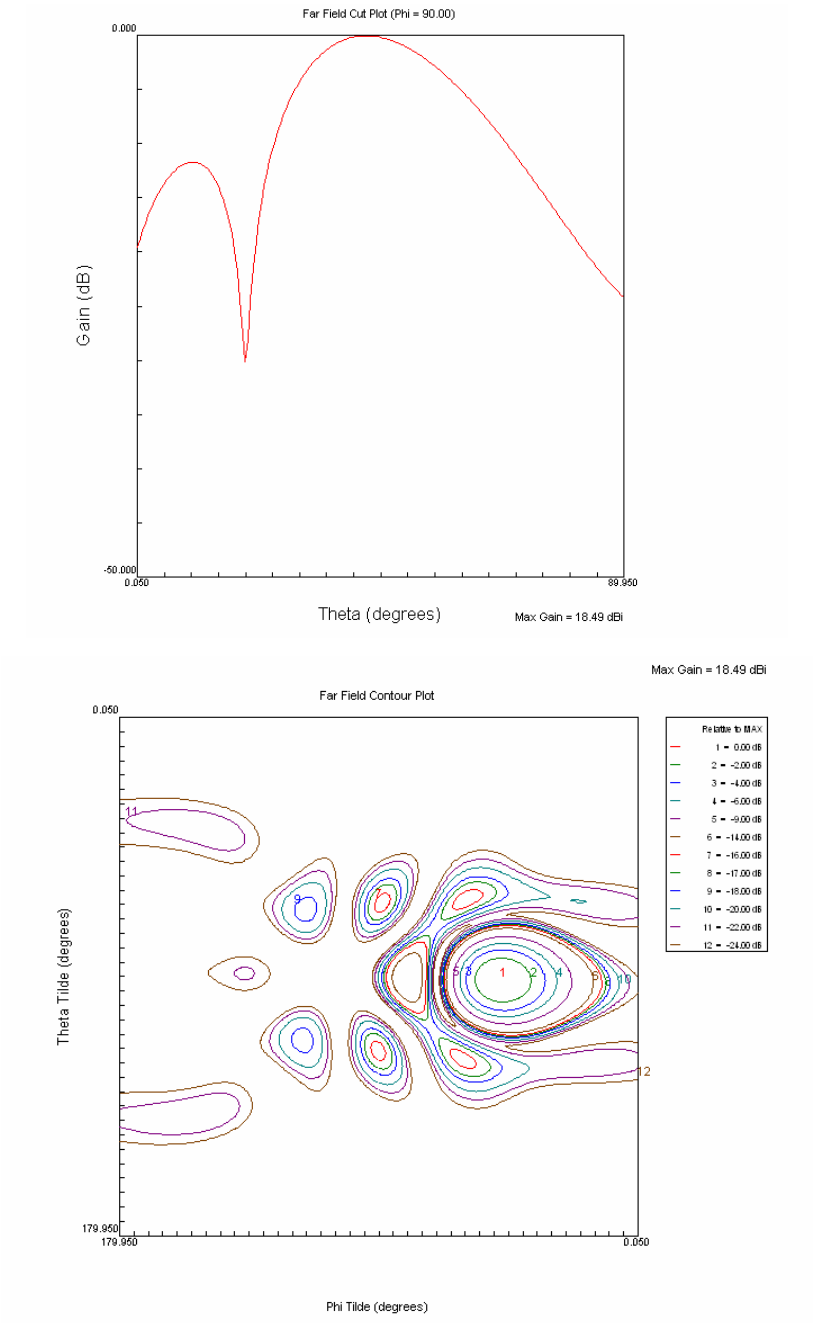

Figure 5.22. 45 Deg, 3 bit Phase-quantized Pattern and Contour Plot for Paraboloidal Array: The gain is 18.49 dB, the SLL is -14 dB.

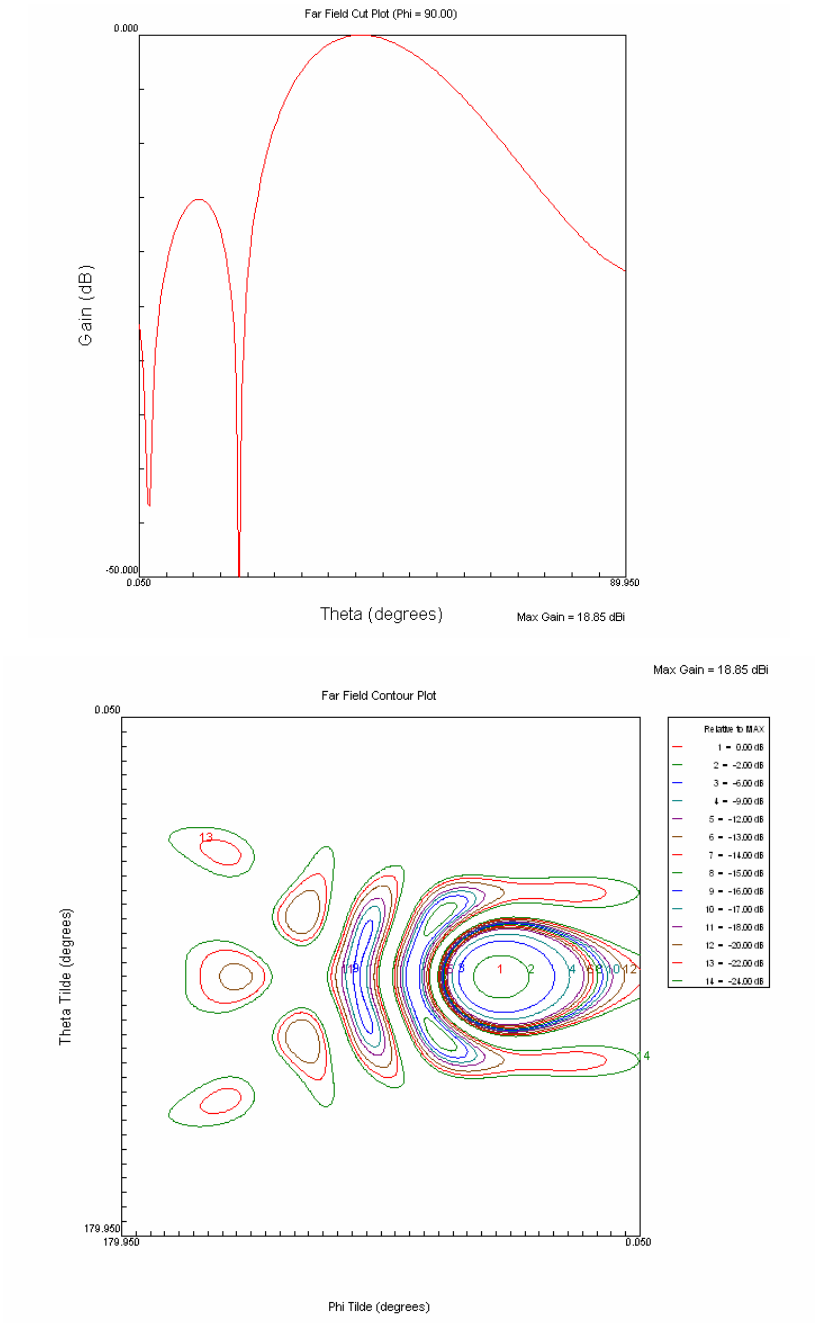

Figure 5.23. 45 Deg, 3 bit Phase-quantized Pattern and Contour Plot for Planar Array: The gain is 18.85 dB, and the SLL is -15 dB.

What is seen in the phase-quantized scans above is that there does not appear to be much degradation in gain in the paraboloidal or planar antennas, as compared to the case where quantization is not used. For scan angles up to 30 degrees, the degradation in gain in the antennas when 4 or 3 bit quantization are used as compared to the non-quantized case is in the order of 0.1 dB or less. When 3 bit phase quantization is used and the arrays scanned beyond 30 degrees, the degradation increases slightly, but remains less than about 0.2 dB for scan angles up to 45 degrees.

We now discuss the variation in side lobe level for the above phase quantized scan angles.

We start with the paraboloidal array. In the case of the paraboloidal array, 4 bit phase quantization applied to scan angles of 15 degrees, 30 degrees, and 45 degrees yields highest side lobe levels of -17 dB, -16 dB, and -14 dB, respectively. In the same array, 3 bit phase quantization applied at the above scan angles gives highest side lobe levels of -18 dB, -16 dB, and -14 dB, respectively. We see, as we would expect, that the highest SLL generally increases with increasing scan angles for both 4 and 3 bit quantizations. We find that the side lobe levels for the phase quantized scans given above are comparable to those derived for the case where no phase quantization was performed.

In the case of the planar array, the scan angles above give us side lobe levels of -16 dB, -15 dB, and -13 dB for 4 bit quantization, and -13 dB, -15 dB, and -15 dB for 3 bit quantization. The side lobe levels thus appear irregular with scan angle when 3 bit phase quantization is performed. Furthermore, we see that the paraboloidal array generally gives better scanned side lobe level performance with phase quantization than the planar array, particularly when 3 bit quantization is used, but also with 4 bit quantization.

The half-power beamwidths of the patterns, as expected, increase with scan angle in both arrays; as the beam is scanned off broadside, it broadens and the gain is diminished. However, the half-power beamwidth is not sensitive to phase quantization level- the beamwidths stay roughly constant with variation in phase quantization at any given scan angle.

In conclusion, phase quantization has a more pronounced effect on side-lobe level than on gain or half-power beamwidth.

5.3 Summary of Simulation Results

Table 5.1 summarizes the simulation results obtained above. The variation of gain, highest side-lobe level, and half-power beamwidth with selected scan angles and phase quantization levels is given for the paraboloidal and planar arrays.

Table 5.1. Summary of Simulation Results

Scan Angle (deg)	**Phase Quantization Level (Bits)**	**Planar Array Gain (dB)**	**Paraboloidal Array Gain (dB)**	**Planar Array SLL (dB)**	**Paraboloidal Array SLL (dB)**	**Planar Array HP Beamwidth (deg)**	**Paraboloidal Array HP Beamwidth (deg)**
0	0	20.35	20.09	-18	-18	18.2	18.3
0	5	20.35	20.05	-18	-18	18.2	18.3
0	4	20.35	20.06	-18	-18	18.2	18.3
0	3	20.35	19.92	-18	-18	18.2	18.3
15	0	20.20	19.91	-16	-17	19	19.2
30	0	19.75	19.44	-15	-16	20.6	20.6
45	0	18.93	18.65	-14	-14	23.7	24
15	4	20.20	19.89	-16	-17	20.5	21
30	4	19.75	19.33	-15	-16	24.1	24.3
45	4	18.97	18.63	-13	-14	28.6	28.5
15	3	20.06	19.84	-13	-18	20.2	21
30	3	19.75	19.42	-15	-16	23.3	22.5
45	3	18.85	18.49	-15	-14	28.6	28.5

The results depicted above show that the paraboloidal array offers performance very similar to that of the planar array. The paraboloidal array offers slightly lower gain than the planar array, but better side lobe level performance.

Chapter 6. Discussion on Mutual Coupling Effects

6.1 Mutual Coupling- Introduction

In analyzing an array, one cannot consider each element to be in electromagnetic isolation from its neighbors. The current on each element in an array influences the currents on all the other elements, thereby altering the pattern of the antenna. Thus, if we desire an accurate analysis of the pattern of an array, we cannot assume that the current on the elements is solely driven by the feed system. The interaction between the elements in an array, called mutual coupling, can be theoretically calculated using numerical methods, such as the Method of Moments.

In general, coupling between elements in an array happens in one of three ways- direct coupling, coupling by reflection off an external object, and coupling through the feed system in the array. Direct coupling depends heavily on the spatial orientation of the elements in the array. For example, the coupling between two parallel dipoles is typically much higher than that between collinear dipoles, due to the stronger direct coupling that occurs in the first case. Coupling by reflection is dependent on the physical environment in which the array operates. Coupling through the feed can be significant in certain types of antennas.

Mutual coupling may be expressed mathematically in one of three ways. It could take the form of an impedance matrix, whereby the voltage at one port due to the current at another port is measured, while keeping the currents at all other ports zero. Another way to express mutual coupling is by means of an admittance matrix, in which each matrix element is simply the reciprocal of the impedance. The third and perhaps most common means is to express it as a scattering matrix, where the reflected “power wave” at a port due to the incident “power wave” at another port is measured. It is possible to mathematically convert mutual coupling expressed in one of the above forms to another.

In this thesis, we will only concern ourselves with mutual coupling in arrays comprised of identical elements, since this is the case in the paraboloidal array under consideration.

6.2 Mutual Coupling in Planar Microstrip Arrays

The primary means by which mutual coupling occurs in microstrip arrays is via surface waves on the antenna substrate. Surface waves not only cause undesired mutual coupling in microstrip arrays, but also reduce the efficiency of the array. More than one mode may be present in the antenna substrate, increasing the complexity of the coupling between elements in the array. As mentioned earlier, mutual coupling each pair of elements in an array may be expressed as an impedance matrix, an admittance matrix, or a scattering matrix. The matrix size for an array of N elements is N^2 x N^2, assuming that only one mode exists in the substrate, since every element in the array is coupled with every other element and obviously itself. If multiple modes M are excited in the substrate, the size of the matrix increases to (M x N^2) x (M x N^2), making the calculations excessively complex. Pozar [8] states, however, that in the case of microstrip arrays, the assumption that only a single mode exists in the substrate yields a reasonable mutual coupling approximation. This is because microstrip patch antennas are inherently resonant structures, and a single mode approximation is quite accurate near resonance.

In [8], the Moment Method is used to derive the mutual coupling, in the form of an impedance matrix, between rectangular patch elements in a planar array. The planar microstrip array configuration shown in Figure 6.1 is studied in [8]:

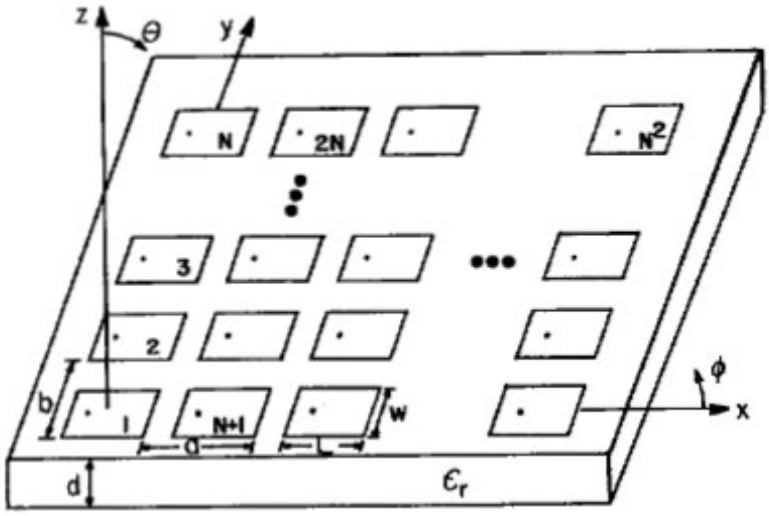

Figure 6.1. Planar Microstrip Array Studied by Pozar

[2006] IEEE. Reprinted, with Permission, from [8]

The mutual impedance equations are as follows [8]:

$$Z_{mn} = jZ0 / 4\pi^2 k_0 \iint Q_{xx}(k_x, k_y)F_x^2(k_x)F_y^2(k_y)\cdot e^{jkxSx}e^{jkySy}\, dk_x\, dk_y \qquad (11)$$

where the integration is performed from - ∞ to ∞. In the above equation,

$Q_{xx}(k_x, k_y) = [\ \{\ (\varepsilon_r k_0^2 - k_x^2)k_2 \cos k_1 d\ + j\ k_1\ (k_0^2 - k_x^2) \sin k_1 d\ \}\ /\ (T_e\ T_m)\ ]\ \sin k_1 d$

and

$T_e = k_1 \cos k_1 d + jk_2 \sin k_1 d$

$T_m = \varepsilon_r k_2 \cos k_1 d + jk_1 \sin k_1 d$

$k_1^2 = \varepsilon_r k_0^2 - \beta^2$, Im $(k_1) < 0$

$k_2^2 = k_0^2 - \beta^2$, Im $(k_2) < 0$

$\beta^2 = k_x^2 + k_y^2$

$k_0 = \omega\sqrt{(\mu_0\varepsilon_0)} = 2\pi / \lambda_0$

$Z_0 = \sqrt{(\mu_0 / \varepsilon_0)}$

$J(x, y) = [\sin k_e (h - |x|)] / W \sin k_e h$, for $|x| < h$, $|y| < W / 2$,

$F_x(k_x) = 2\ k_e\ (\cos k_x h - \cos k_e h) / \sin k_e h(k_e^2 - k_x^2)$,

$F_y(k_y) = [\sin k_y W/2] / (k_y W/2)$

The impedance equation above is very general in that it gives the mutual impedance between two modes m and n, where multiple modes might exist on each port. In the equations above, W is the patch width (and the width of the mode), S_x and S_y are the distances in x and y separating the two modes m and n, h is the half-length of the mode, and k_e is the effective wavenumber of the mode.

The computational effort required to derive the mutual coupling in a microstrip array is evident in the above equation. It is generally assumed that there is only one dominant mode at each port to simplify the above equations.

While equation (11) is for a planar array comprised of rectangular patches, the paraboloidal array we are considering is comprised of circular patches. The mathematical form of the equations for our case would thus be different, but the above equations are instructive nonetheless. However, the computational complexity of finding the mutual

impedance in the paraboloidal array would be far greater, due to the varying orientations of the elements.

In the next section, we consider the mutual coupling between elements when they are located on a curved surface, such as a paraboloid.

6.3 Mutual Coupling in Conformal Arrays

The calculation of coupling between elements in a planar array is typically much simpler than that for a conformal array. In a planar array, the calculation of mutual coupling is essentially a two-dimensional problem rather than a three-dimensional problem, as is the case for a conformal array. Mutual coupling in a conformal array is consequently much more sensitive to the polarization of the elements. In a conformal array, the direct coupling between elements depends not just on the distance between the elements, as is primarily the case in a planar array, but on the spatial configuration of the elements as well.

Persson et al [9] studied the mutual coupling between elements located on a doubly curved convex surface. We note here that the paraboloidal array that is the subject of our thesis is located on a doubly curved concave surface, and not a convex surface. A doubly curved surface is one that exhibits curvature in both horizontal and vertical planes, and is the most general type of curved surface. The paraboloidal surface on which the phased array under consideration in this thesis is located is a doubly curved surface.

The coupling between apertures located on the convex side of a paraboloidal surface was studied in [9]. We emphasize once more that the results obtained by Persson et al are applicable to the convex side of a paraboloidal surface, and are therefore different from what we would expect in our case (the concave side of the paraboloid). In fact, the coupling between elements located on the concave side of a paraboloid would be considerably greater than that between elements located on the convex side, due to increased alignment of element polarizations. However, studying the results that Persson et al get is instructive nonetheless, since both surfaces are doubly curved paraboloids. Persson et al derived a general expression for mutual coupling between apertures on such a doubly curved surface in the form of an admittance matrix. This equation is general enough that it

is applicable to the (concave) paraboloidal array as well. Each element in the admittance matrix is given by [9]:

$$Y_{pi}^{qj} = [\iint_{Sp} (E_p (e_p^q) \times H_p (e_i^j)) \cdot n_p \, dS] / (V_p^q \, V_i^j) \quad (12)$$

This electric and magnetic field-based equation represents an alternative but equivalent way to express mutual coupling to that typically used, which involves voltages and currents at ports. The equation expresses the mutual admittance between ports i and p, and modes j and q. Mode j is present on port i, and mode q is present on port p. The mode j present on port i will result in a magnetic field to appear at port p. In addition, port p will also have an electric field due to the mode q present on it. The cross product of the electric and magnetic fields present on port p due to the modes present on the two ports gives us the power in the port, but also a measure of a the coupling between the two different ports and modes. The double integral in the numerator effectively calculates the power present at a port due to coupling with a different port, taking into account the possibility of different modes being present in each port. The denominator is the product of the two voltages at the two ports, each depending on the mode excited on it. Thus, a voltage exists at port p due to the mode q that exists on it, and a voltage exists at port i due to the mode j that exists there. Since impedance may be expressed as $Z = V^2 / \text{Power}$, where V is voltage, admittance $Y = \text{Power} / V^2$, as the equation above clearly states. The double integral in the numerator is performed over the aperture surface S_p, and the curvature of the paraboloid is taken into account in the dot product with the unit normal port vector n_p and integration over the port surface. The equation above thus expresses the mutual coupling, in the form of an admittance matrix, between elements in a phased array in the most general case possible, in which the array surface is doubly curved and multiple modes may exist in the different ports.

To verify the accuracy of his theoretical expression, Persson et al used an antenna built by Ericsson Microwave Systems for experimentation and comparison with the theoretical results obtained with his admittance expression. The antenna consisted of 48 circular-wavegude-fed apertures located on a convex paraboloidal surface. In his experiments on coupling, he designated one of the 48 apertures as the source, and several of the remaining apertures as observation apertures, and measured the scattering parameters

for each pair of source-observation apertures. To study the polarization-sensitivity of mutual coupling between apertures on a curved surface, [9] used all four combinations of two orthogonal linear polarizations on the source and the observation apertures. The two orthogonal polarizations used were radial and angular. For example, the source may be radially polarized and the observation aperture angularly polarized in one measurement, and vice versa in another. The two orthogonal polarizations were implemented by simply rotating the waveguides feeding the apertures. As expected, it was found that mutual coupling is highly distance-dependent in each case, and that moreover, it is also sensitive to polarization in a complex way.

Persson et al also compared the results obtained from measurements with those obtained using his theoretical model, and found them to agree very closely in all cases. The results in [9] are summarized in the plots that follow.

Figure 6.2 shows the configuration of the aperture elements used in [9]; they are strategically placed on a convex paraboloid.

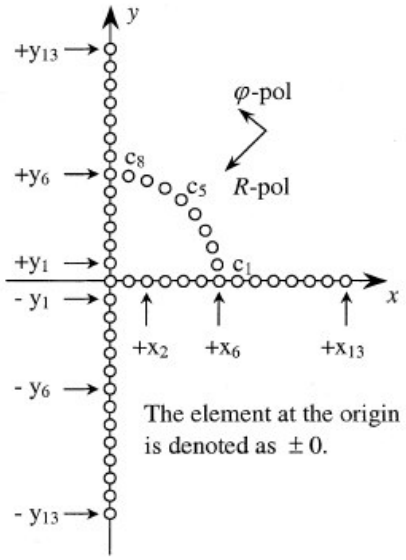

Figure 6.2. Configuration of Apertures on Convex Paraboloid Studied by Persson

[2006] IEEE. Reprinted with permission from [9]

The photo and diagram shown in Figure 6.3 are of the experimental convex paraboloidal antenna built in [9].

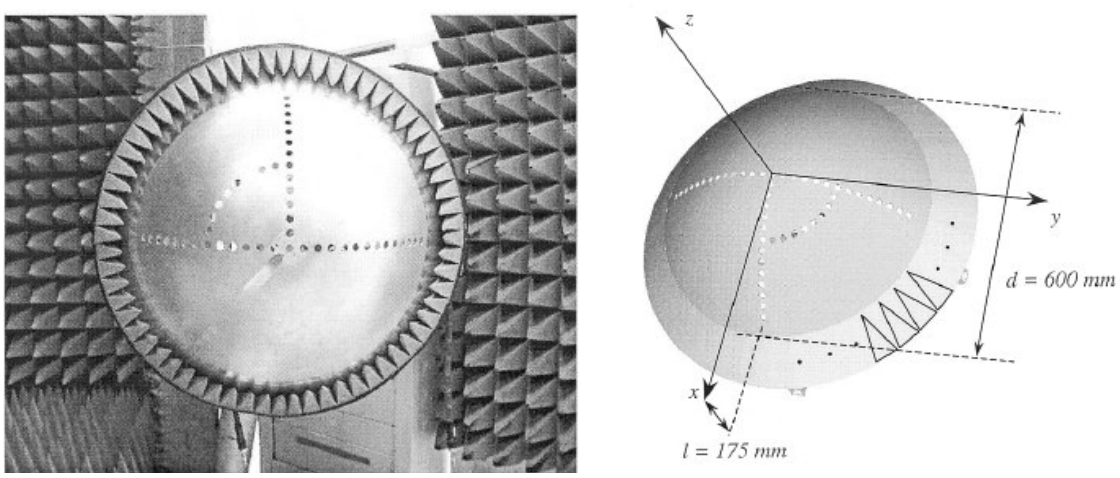

Figure 6.3. Convex Paraboloidal Aperture Array Studied by Persson

The table below lists the different combinations of [observation aperture, source aperture] polarizations studied, and specifies the source elements and the receiving elements.

Table 6.1. Cases Studied by Persson et al

Source Element	**Receiving Elements**	**Polarization**
$-y_{13}$	Along the y-axis, ie. $-y_{12}$ to $+ y_{12}$	[R,R]
$-y_{13}$	Along the first part of the y-axis, ie. $-y_{12}$ to $- y_8$	[R, φ]
$-y_{13}$	Along the first part of the y-axis, ie. $-y_{12}$ to $-y_8$	[φ, R]
$-y_{13}$	Along the y-axis, ie. $-y_{12}$ to $+ y_{12}$	[φ, φ]
$+ x_6$	Along the circle arc, ie. c_1 to c_8 and $+y_6$	All four Comb.
c_5	Along the positive y-axis, ie. +/- 0 to $+ y_{12}$ For the [φ,φ]-case, the negative y-axis was included in the calculations	All four Comb.

We now show some selected results in [9]. The plots in Figures 6.4 and 6.5 depict the variation of mutual coupling (in the form of scattering parameters) with respect to

source and observation apertures- both measured values, and values calculated using the equation presented earlier, are shown.

Figure 6.4 is the plot for the case where both source and observation aperture are radially polarized; also shown is a diagram depicting the source and observation points in the antenna. The vertical axis is the scattering parameter in dB, and the horizontal axis denotes distance.

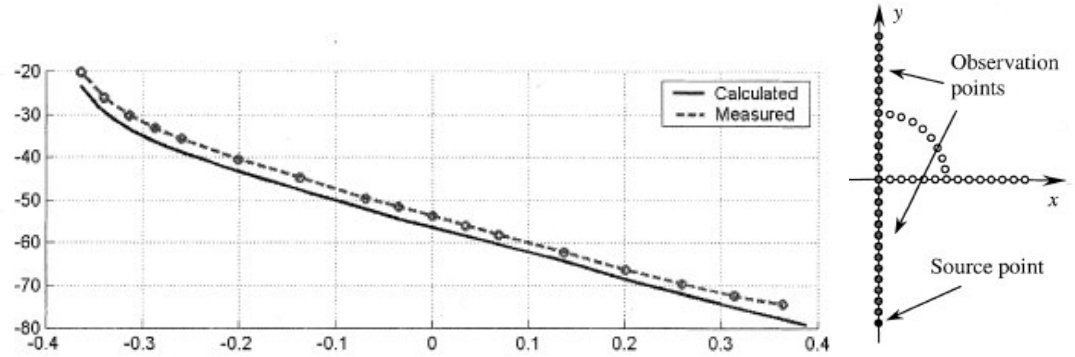

Figure 6.4. Plot of Mutual Coupling (dB) versus Distance for Radial Polarization

It can be seen from the plot in Figure 6.4 that the mutual coupling decreases steadily with inter-element distance.

In Figure 6.5, the source is angularly polarized, but the observation apertures are radially polarized.

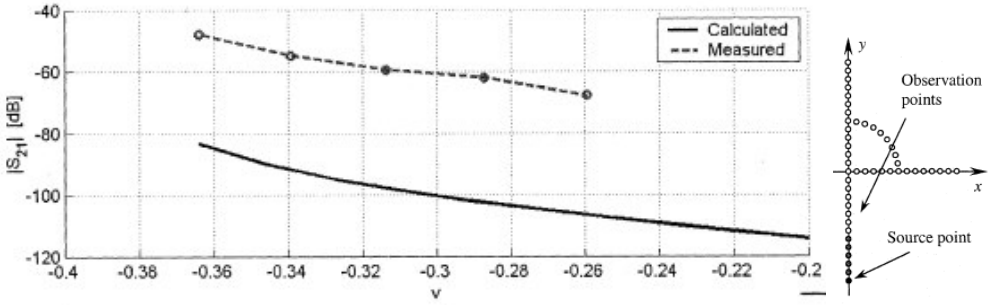

Figure 6.5. Plot of Mutual Coupling (dB) versus Distance for Mismatched Polarizations

As can be seen above, the mutual coupling has decreased dramatically when compared to the case where both source and observation apertures were radially polarized. This reduction in mutual coupling occurs due to the orthogonality of the source and observation aperture polarizations.

Figures 6.6 and 6.7 show a more complex dependence of mutual coupling on polarization.

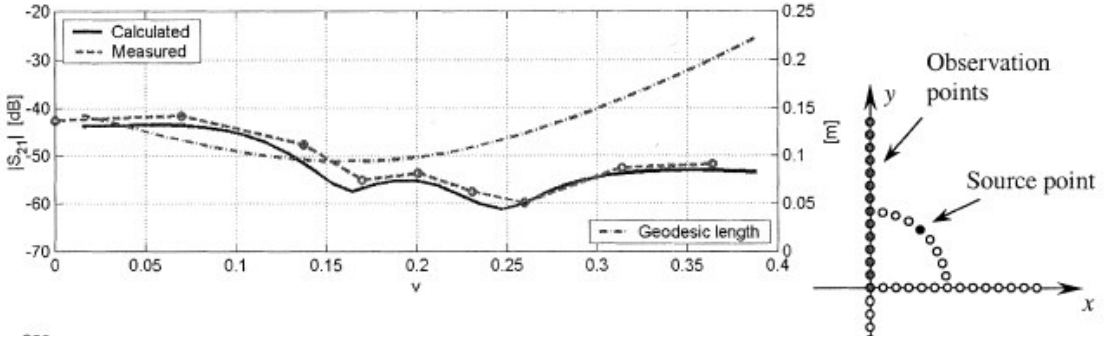

Figure 6.6. Plot of Mutual Coupling (dB) versus Distance for Radial Polarizations

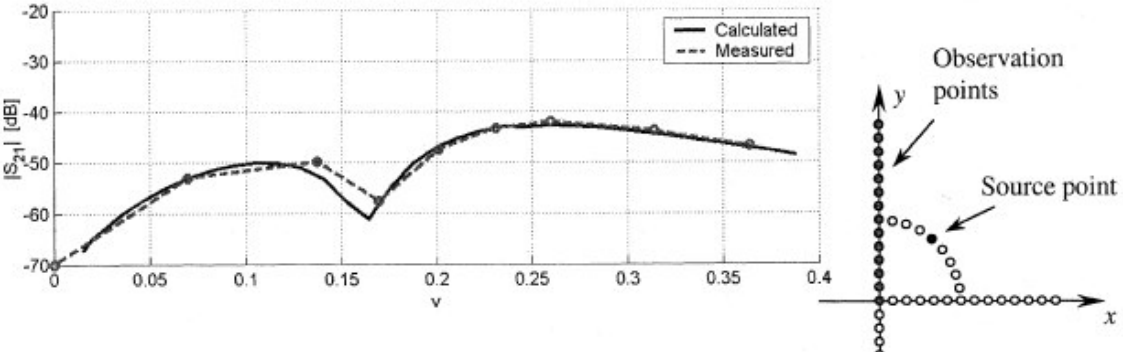

Figure 6.7. Plot of Mutual Coupling (dB) versus Distance for Angularly Polarized Source and Radially Polarized Observation Points

[2006] IEEE. Figs. 6.3-6.7 reprinted with permission from [9]

The increased complexity observed in the plots is attributable in part to the variations in the alignments of the polarizations of the source and observation apertures, due to their being located on a curved surface. Polarization dependence of mutual coupling in a planar array is much simpler, because of its two-dimensional nature.

We would intuitively expect that the mutual coupling would be much stronger in the concave paraboloidal array than was the case in the convex array. Elements located on a concave paraboloid face each other to some extent, and there is consequently strong direct coupling between elements, whereas on a convex paraboloid, elements face away

from each other, reducing direct coupling. Figure 6.8 illustrates this point.

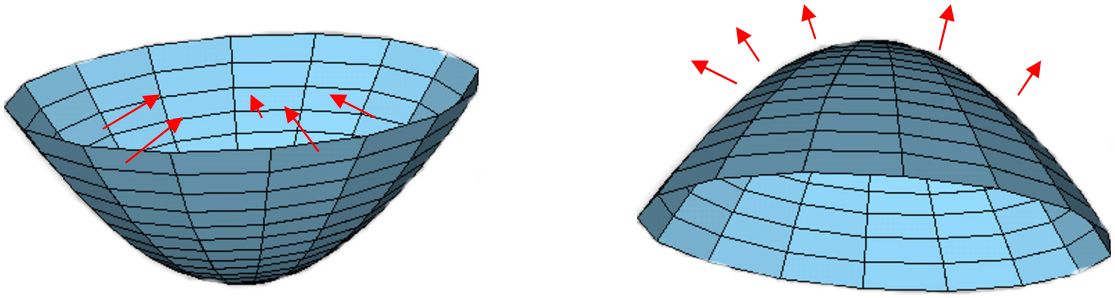

Figure 6.8. Illustration of Difference in Direct Mutual Coupling Between Convex and Concave Paraboloidal Arrays

We would thus expect there to be relatively strong coupling between elements in the paraboloidal array, and a significant and complex dependence on element polarization as well.

Chapter 7. Beam-Forming Feed Network

7.1 Background on Microstrip Feed Networks

Microstrip lines constitute the feed network used to excite each element in the array. Feed network design is dictated by the required relative phases and amplitudes of the electromagnetic waves radiated by each element in the array. Before further discussing the feed network, we first clearly define the relative phases and amplitudes desired at each element. If we want the array to have the maximum possible gain, each element must be fed with an equal excitation current. Furthermore, we want the phases of the radiated electromagnetic waves from all the elements to be uniform, so as to produce the maximum radiation in a broadside direction. Since the elements conform to a paraboloidal (non-planar) surface, patches located at different distances from the paraboloid's center radiate waves that are out of phase with each other in the far field due to the differences in the distance traveled by each wave. The feed excitation at each element must compensate for this non-uniform far field phase distribution by imposing non-uniform phases for elements located at different distances from the paraboloidal center. In designing the feed network, we must also provide impedance matching between each element and the feed network, as well as within the feed network, to prevent reflections.

To ensure that each element in the array is fed with an equal excitation current, the impedance of the microstrip lines feeding the elements must be the same. We can achieve a uniform phase distribution for elements located at equal distances from the paraboloid's center by ensuring that the microstrip lines feeding each element are of equal length. To implement impedance matching at an element, the microstrip line feeding a patch must have the same impedance as the patch. Furthermore, impedance matching within the feed network is achieved by using microstrip lines of different widths, such that at a point where a single line divides into two, the parallel combination of the impedance of the two lines is equal to that of the single line.

A commonly used microstrip feed network that satisfies all of the above requirements is the parallel or corporate feed network. Such a feed network is characterized by successive divisions of a microstrip line to connect to the patch elements in parallel. The

symmetry inherent in a parallel feed ensures that the current delivered to each patch has the same amplitude and phase. A corporate microstrip feed network, like any feed network, will result in a certain amount of loss of antenna efficiency and gain, due to losses in the microstrip lines, undesired radiation from the lines, and mutual coupling between patches via surface waves.

7.2 Proposed Microstrip Feed Network Design

A corporate feed network is chosen to feed the elements in the paraboloidal array. Following is a brief description of the entire proposed antenna configuration, including the feed network. The uppermost layer of the antenna consists of the radiating layer, where all the array elements are located. Beneath the array elements is a layer of dielectric material, and below that, the ground plane. Underneath the ground plane is located another layer of dielectric material, followed finally with the feed matrix layer as the bottommost layer. The feed network layer is comprised not only of the feed network, but also the phase shifters, and any attenuators that we may wish to employ in the design. Holes in the feed network layer and the ground plane facilitate electromagnetic coupling to the radiating array layer. Alternatively, probe feeding of the radiating elements could also be used.

The central element in the array was not fed by the beam-forming feed network, since this element would be used to feed the hyperbolic subreflector in the hybrid antenna (see section on Future Work). The beam-forming network must feed the remaining 36 elements in the paraboloidal array. There are a number of ways that we can use to design the beam-forming network for these elements; the approach that we chose was to implement a network utilizing two 2-way power dividers and two 3-way power dividers, so as to feed all 36 elements. The antenna elements were grouped into convenient units of three elements, exploiting the symmetry of the hexagonal array to design a relatively simple microstrip beam-forming network. Figures 7.1 to 7.5 show the beam-forming network; first, we show the network in its entirety, and then we show the step-by-step process by which the feed network was designed so as to make the antenna groupings clear.

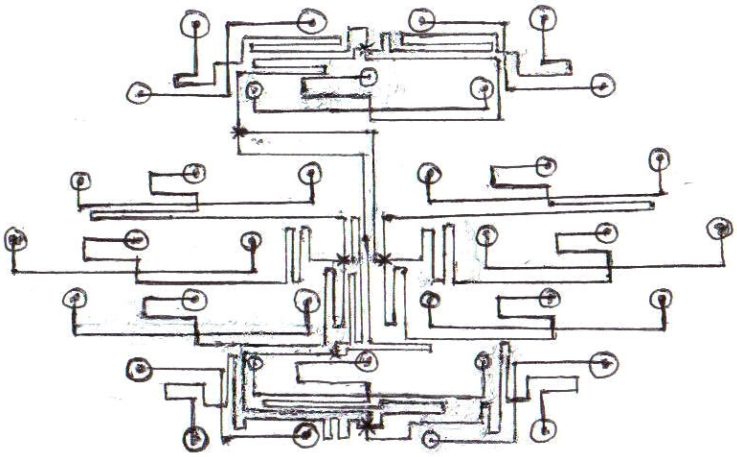

Figure 7.1. Schematic of Beam-forming Network

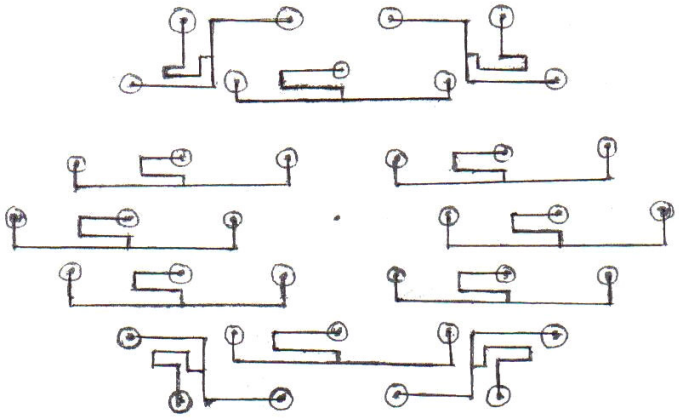

Figure 7.2. Schematic of Beam-forming Network: Groupings of 3 Elements

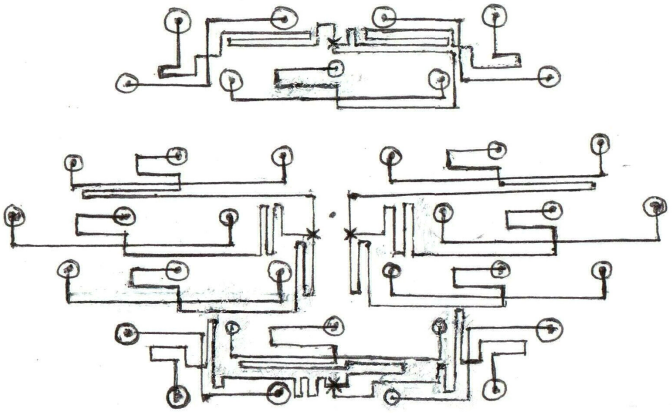

Figure 7.3. Schematic of Beam-forming Network: Groupings of 9 Elements

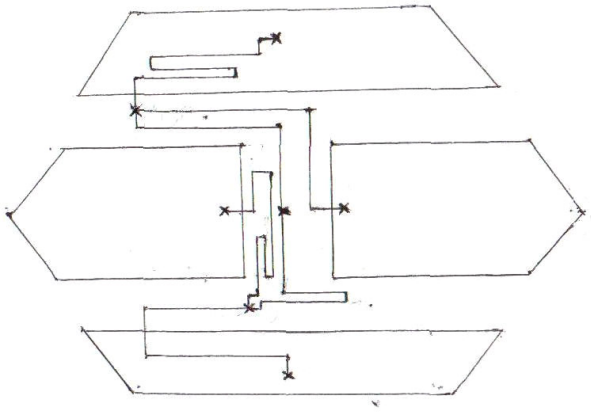

Figure 7.4. Schematic of Beam-forming Network: Connections between 9 Element Groupings

From the diagrams above, it is seen that equal line lengths are implemented to each element, in a typical corporate feed configuration.

The corporate feed network schematic depicted above is shown in Figure 7.5 with microstrip line impedances labeled.

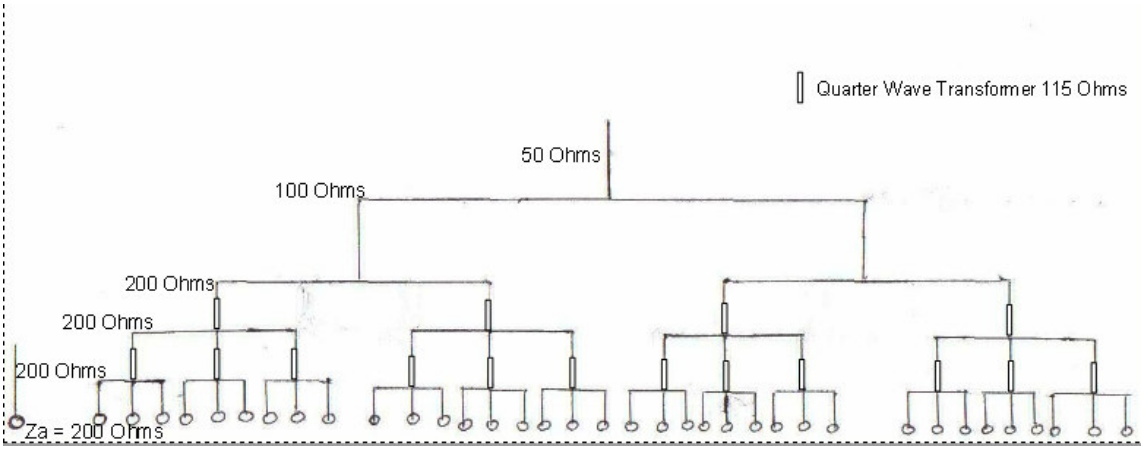

Figure 7.5. Feed Network Diagram with Line Impedances

The element impedance is assumed to be 200 ohms, so that the impedance of the mircostrip line feeding the antennas must be 200 ohms as well. Quarter wave transformers (depicted as rectangles along the microstrip lines at the point of division) are needed to match impedances in the third and fourth stages of the network. The parallel combination of three 200 ohm lines gives an impedance of 66.7 ohms, which must be matched to the 200 ohm line feeding them; the required transformer impedance is
$\sqrt{}$ (66.7 x 200) = 115 ohms. The input impedance of the entire microstrip feed network is 50 ohms, and all microstrip lines are matched. The left-most antenna and microstrip line depicted is separate from the beam-forming feed network, and feeds the hyperbolic subreflector in the hybrid antenna configuration.

Chapter 8. Conclusions and Future Work: Hybrid Reflector-Array Antenna

The simulation results and analysis in this thesis have shown that a phased array of circular microstrip patches conformal to a paraboloidal surface yields similar scan performance with respect to gain, side-lobe level, and HP beamwidth to a planar array. The paraboloidal array has a slightly lower gain than the planar array, but has better side lobe level performance with scanning when phase quantization is implemented. Both arrays generally show a SLL increase of 1 dB per 15 degrees of variation in scan angle with no phase quantization implemented. The half-power beamwidth of the array increases with scan angle as expected. Phase quantization has minimal effects on the gain and beamwidth of the paraboloidal array, and has a more adverse impact on the side-lobe level of the planar than the paraboloidal array. In general, a slight increase in side-lobe levels occurs with higher bit phase quantization, particularly at larger scan angles.

A simple corporate microstrip beam-forming feed network has been designed for the paraboloidal array. Consideration of mutual coupling in the paraboloidal array indicates a heavy dependence on polarization.

This thesis provided a general discussion of mutual coupling in the paraboloidal array, but rigorous coupling analyses and calculations were not within its scope. A more intensive treatment of mutual coupling in the paraboloidal array could be the subject of a new thesis. Such a comprehensive treatment of mutual coupling in the paraboloidal array would have to combine aspects of the studies done by Pozar and Persson on mutual coupling in planar microstrip patch arrays and conformal arrays, respectively. The electric field at a patch due to the presence of neighboring patches would have to be calculated using a variant of Pozar's methods, such that the curvature of the paraboloidal surface is accounted for. Then, Persson's method for finding mutual coupling in a conformal array could be applied. It should be noted that an exhaustive treatment of mutual coupling in the paraboloidal array is expected to be a significant undertaking, and could constitute a thesis or dissertation.

The paraboloidal array that was described in this thesis is to be part of a hybrid antenna, comprised of a parabolic reflector antenna placed behind the array, and the

reflector fed by the central element(s) of the array via a hyperbolic subreflector in a Cassegrain configuration [10]. Thus, the proposed hybrid antenna is a standard Cassegrain dual reflector with the paraboloidal array located in front of the primary reflector surface. Such a hybrid antenna will allow us to use both the scanning capabilities of the paraboloidal array and the broadside beam of the reflector simultaneously, effectively making it two antennas in one. Additionally, we could use the array to transmit and the reflector to receive, or vice versa, or operate them at two different frequencies at the same time. Such a flexible antenna would find application in environments where space is at a premium.

References:

[1] "ARRAY Manual", COMSAT Laboratories, 1997.

[2] W. Stutzman and G. Thiele, "Antenna Theory and Design", John Wiley & Sons, Inc., 1998.

[3] D.M. Kokotoff et al, "Figure of Merit for the Design of Microstrip Patch Antennas".

[4] C.A. Balanis, "Antenna Theory", John Wiley & Sons Inc., 1997.

[5] A. Forenza et al, "Pattern Diversity with Multi-mode Circular Patch Antennas in Clustered MIMO Channels".

[6] A.K. Verma and Nasimuddin, "Simple and Accurate Expression for Directivity of Circular Microstrip Antenna", Journal of Microwaves and Optoelectronics, Vol. 2. No. 6, December 2002.

[7] S Hara et al, "Acceleration of Beamforming Speed for RF MEMS-Implemented Phased Array Antenna, 2003.

[8] D.M. Pozar, "Finite Phased Arrays of Rectangular Microstrip Patches", IEEE Transactions on Antennas & Propagation, Vol. AP-34, No. 5, May 1986.

[9] P. Persson, "Investigation of the Mutual Coupling Between Apertures on Doubly Curved Convex Surfaces: Theory and Measurements", IEEE Transactions on Antennas and Propagation, Vol. 51, No. 4, April 2003.

[10] A.I. Zaghloul and B.A. Pontano, "Hybrid Reflector-Array Antenna Concept," IEEE International Symposium on Antennas and Propagation, Alburquerque, NM, July 2006.

[11] D.M. Pozar, "Input Impedance and Mutual Coupling of Rectangular Microstrip Antennas", IEEE Transactions on Antennas and Propagation, Vol. AP-30, No. 6, November 1982.

[12] M. Parsa, "Simulation of Antenna Array Conformal to a Parabolic Reflector", Masters Degree Final Examination, May 2006.

[13] M.E. Bialkowski and N.C. Karmakar, "A Two Ring Circular Phased Array Antenna for Mobile Satellite Communications", IEEE Antennas & Propagation Magazine, Vol. 41, No. 3, June 1999.

Vita

Sharath Kumar was born in Jamshedpur, India. He received his B.S. in Electrical Engineering from Virginia Tech, Blacksburg in 2001, and worked as a Systems Engineer at Northrop Grumman until 2004. He enrolled in Virginia Tech as a graduate student in 2004 at the National Capital Region campus in Falls Church, Virginia. This thesis fulfils the requirements for his M.S. in Electrical Engineering.